© 2021. Published by The Company of Biologists Ltd | Development (2021) 148, dev199584. doi:10.1242/dev.199584

RESEARCH ARTICLE

Live imaging of retinotectal mapping reveals topographic map dynamics and a previously undescribed role for Contactin 2 in map sharpening

Olivia Spead, Cory J. Weaver, Trevor Moreland and Fabienne E. Poulain*

ABSTRACT

Organization of neuronal connections into topographic maps is essential for processing information. Yet, our understanding of topographic mapping has remained limited by our inability to observe maps forming and refining directly *in vivo*. Here, we used Cre-mediated recombination of a new colorswitch reporter in zebrafish to generate the first transgenic model allowing the dynamic analysis of retinotectal mapping *in vivo*. We found that the antero-posterior retinotopic map forms early but remains dynamic, with nasal and temporal retinal axons expanding their projection domains over time. Nasal projections initially arborize in the anterior tectum but progressively refine their projection domain to the posterior tectum, leading to the sharpening of the retinotopic map along the antero-posterior axis. Finally, using a CRISPR-mediated mutagenesis approach, we demonstrate that the refinement of nasal retinal projections requires the adhesion molecule Contactin 2. Altogether, our study provides the first analysis of a topographic map maturing in real time in a live animal and opens new strategies for dissecting the molecular mechanisms underlying precise topographic mapping in vertebrates.

KEY WORDS: Visual system, Zebrafish, Axon guidance, Refinement, Adhesion molecule

INTRODUCTION

Organization of neuronal connections into topographic maps facilitates the efficient transfer of information between brain regions. In the visual system, retinal projections transmit a continuous representation of the external world by maintaining the neighboring relationship of the neurons they originate from in the retina (Cang and Feldheim, 2013; Triplett, 2014). Along the antero-posterior (A/P) axis, retinal ganglion cells (RGCs) in the nasal retina project axons to the posterior optic tectum [or superior colliculus (SC) in mammals], whereas temporal RGCs innervate the anterior tectum. As Sperry first postulated in his chemoaffinity hypothesis (Sperry, 1963), studies in mouse, chick, *Xenopus* and fish have demonstrated that this precise retinotopic map is first established by specific axon-target interactions, whereby axons with a specific set of receptors interpret guidance cues distributed in a gradient at the target. Subsequently to this guidance process, retinotopic projections are refined by activity-dependent mechanisms triggered by spontaneous retinal activity or visual experience (Kutsarova et al., 2016; Leighton and Lohmann, 2016; Thompson et al., 2017).

It is now well accepted that both guidance cues at the target and patterned retinal activity act together to establish a precise retinotopic map (Benjumeda et al., 2013; Cang et al., 2008; Pfeiffenberger et al., 2006). However, other mechanisms such as repulsive, competitive and stabilizing interactions among axons themselves also participate in initial mapping and refinement (Gosse et al., 2008; Hua et al., 2005; Louail et al., 2020; Rahman et al., 2020; Spead and Poulain, 2020a; Suetterlin and Drescher, 2014; Weth et al., 2014). Yet, our understanding of how and when trans-axonal signaling contributes to retinotopic mapping has remained limited by our inability to selectively manipulate RGCs in a topographic manner. It also remains unclear how the retinotopic map becomes sharper as a whole, as we currently lack the ability to observe the map forming and refining over time in the same embryo *in vivo*. Retinotopy can be analyzed at early stages by injecting lipophilic dyes or electroporating DNA in specific retinal quadrants. However, both approaches often require fixing specimens for analysis and have some degree of variability, which precludes the study of mapping dynamics and the detection of subtle topographic changes between times or conditions.

Because of its rapid external development and transparency, the zebrafish larvae has become a model of choice for studying retinotopy (Förster et al., 2020; Poulain et al., 2010). Injection of lipophilic dyes in opposite retinal halves has been used extensively to label retinotopic projections during development or regeneration and identify mutants with retinotopic defects (Baier et al., 1996; Harvey et al., 2019; Stuermer, 1988; Trowe et al., 1996; Xiao et al., 2005). Using that approach, early studies have shown that nasal and temporal retinal axons are localized at retinotopic sites as early as 3 days post-fertilization (dpf), with temporal and nasal axons innervating the anterior and posterior tectum, respectively (Stuermer, 1988; Stuermer et al., 1990). Labeling a subset of RGCs in larvae fixed at 4 and 6 dpf has also revealed that projections cover a smaller territory at later stages, suggesting a refinement of the retinotopic map over time (Gnuegge et al., 2001). That reduced coverage is not observed in larvae treated with the voltage-gated sodium channel blocker tetrodotoxin, indicating a role for neuronal activity in retinotopic map maturation. Although these observations highlight similar mechanisms underlying precise retinotopy in zebrafish and other species, we still do not know exactly when and how the retinotopic map sharpens and matures in teleosts. Advances in molecular genetics have allowed the generation of multiple transgenic lines for analyzing the lineage and functions of neuronal populations in zebrafish (Kawakami et al., 2016; Portugues et al., 2013; Robles, 2017), but the lack of enhancers driving transgene expression in specific retinal quadrants has precluded a similar unbiased analysis of retinotopic mapping over time *in vivo*.

Department of Biological Sciences, University of South Carolina, Columbia, SC 29208, USA.

*Author for correspondence (fpoulain@mailbox.sc.edu)

F.E.P., 0000-0002-7867-748X

Handling Editor: Steve Wilson
Received 3 March 2021; Accepted 7 October 2021

Development (2021) 148, dev199584. doi:10.1242/dev.199584

Here, we report the generation of the first genetic model allowing the dynamic and quantitative analysis of retinotopic map formation and refinement directly *in vivo*. We show that an enhancer located upstream of *hmx1* on chromosome 1 drives selective transgene expression in the nasal retina throughout development. We used Cre-mediated recombination of an *RGC:colorswitch* reporter to specifically label nasal and temporal retinal axons *in vivo* and image their projection domains at the tectum from 3 to 6 dpf by live confocal microscopy. Our analysis reveals that the A/P retinotopic map forms early but remains dynamic, with nasal and temporal axons expanding their projection domains over time. We further show that nasal projections initially arborize in the anterior half of the tectum but progressively refine and condense their projection domain to the posterior tectum from 4 to 5 dpf. That refinement coincides with a sharpening of the retinotopic map along the A/P axis. We finally demonstrate that the adhesion molecule Contactin 2 (Cntn2) is required for the refinement of nasal projections. Altogether, our study provides the first analysis of a topographic map maturing in real time in a live animal and identifies Cntn2 as a previously undescribed regulator of retinotopic map sharpening in vertebrates.

RESULTS

hmx1 is expressed in the nasal retina throughout development

To identify potential enhancers that would drive specific expression in the nasal or temporal retina in zebrafish, we first assessed genes that were previously reported to be regionally expressed in the retina. Among them, the transcription factor *hmx1* has been specifically detected in the nasal retina of several vertebrates (Boisset and Schorderet, 2012; Schulte and Cepko, 2000; Takahashi et al., 2003; Yoshiura et al., 1998). Given its role in retinal patterning, we decided to further analyze and quantify *hmx1* expression throughout retinotectal development by *in situ* hybridization (ISH). At 24 h post-fertilization (hpf), when optic cup morphogenesis is complete (Kwan et al., 2012), *hmx1* was strongly expressed in the nasal retina and lens and was also faintly detected in the otic vesicle (Fig. 1A,A′). At 48 hpf, when first retinal axons reach the tectum (Burrill and Easter, 1995; Stuermer, 1988), *hmx1* remained strongly expressed in the nasal retina and otic vesicle and could also be detected in the pharyngeal arches (Fig. 1B,B′,E). Interestingly, although *hmx1* expression remained stable in the otic vesicle and pharyngeal arches over time, it became restricted to the RGC layer in the nasal retina at 72 hpf (Fig. 1C,C′,F) and 96 hpf (Fig. 1D,D′,G). *Hmx1* expression could also be detected at lower levels in the nasal inner nuclear layer at both stages (Fig. 1F,G). We further quantified *hmx1* expression levels in the RGC layer along a 360° clockwise trajectory at 48, 72 and 96 hpf (Fig. 1H) and found a sharp gradient of expression along the nasal-temporal axis, with *hmx1* being highly expressed in the nasal half of the retina but absent from the temporal half at all three stages (Fig. 1I). As *hmx1* and its paralog *hmx4* arose from tandem duplication and are tightly linked on the same chromosome in chick and zebrafish (Adamska et al., 2001; Wotton et al., 2009), we also

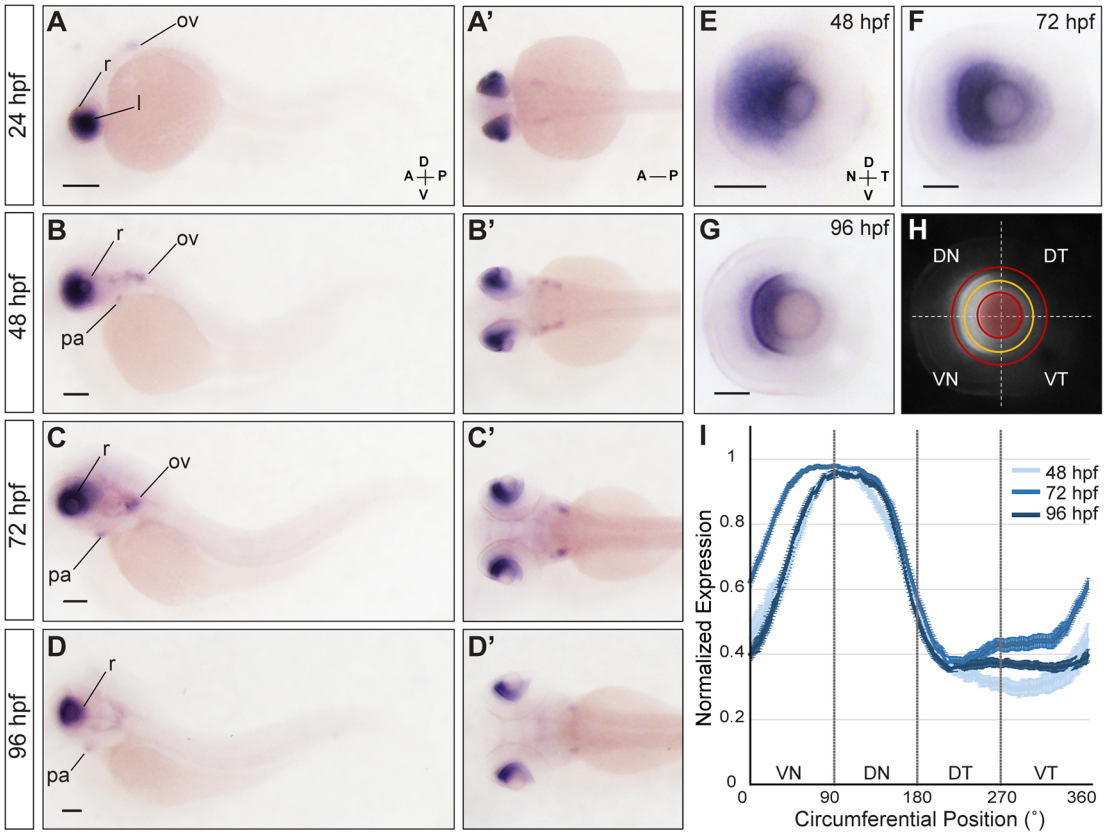

Fig. 1. *Hmx1* is expressed in the nasal RGC layer throughout development. (A-D′) Lateral (A-D) and dorsal (A′-D′) views of embryos stained for *hmx1* by ISH. *Hmx1* is detected in the nasal retina (r), lens (l), otic vesicle (ov) and pharyngeal arches (pa) at 24 hpf (A,A′), 48 hpf (B,B′), 72 hpf (C,C′) and 96 hpf (D,D′). (E-G) Dissected eyes stained for *hmx1*. *Hmx1* is detected in the nasal half of the retina at 48 hpf (E) and becomes restricted to the nasal RGC and inner nuclear layers at 72 and 96 hpf (F,G). (H) *Hmx1* expression signal intensity was measured along a 360° trajectory line (yellow) drawn half-way between the lens and RGC layer periphery (red lines). (I) *Hmx1* expression is restricted to the nasal RGC layer. Data are mean±s.e.m. DN, dorso-nasal; DT, dorso-temporal; VN, ventro-nasal; VT, ventro-temporal. Scale bars: 200 µm (A-D′); 50 µm (E-G).

Development (2021) 148, dev199584. doi:10.1242/dev.199584

analyzed the expression of *hmx4* during retinal development (Fig. S1). As previously described in chick (Deitcher et al., 1994; Schulte and Cepko, 2000), *hmx4* had a similar expression to that of *hmx1* and was strongly detected in the nasal retina from 24 to 96 hpf.

A distal *hmx1* enhancer drives selective expression in nasal progenitors and RGCs

The restricted expression of *hmx1* and *hmx4* in the nasal retina prompted us to search for potential enhancers regulating their expression. Transcriptional enhancers are cis-regulatory elements containing short DNA sequences bound by specific transcription factors. Their activity has been correlated with the enrichment of specific post-translational modification of histones, allowing the prediction of their position in the genome. Active enhancers are notably associated with the presence of histone H3 lysine 4 monomethylation (H3K4me1) and H3K27 acetylation (H3K27ac), whereas H3K4me3 is predictive of active promoters (Bonn et al., 2012; Heintzman et al., 2007; Rada-Iglesias et al., 2011). We thus analyzed the genomic tracks of H3K4me3, H3K4me1 and H3K27ac modifications previously generated by Bogdanovic et al. (2012) to identify putative distal regulatory elements in the *hmx1/4* locus region on chromosome 1 (Fig. 2A). We identified three regions that were characterized by the genomic co-localization of H3K4me1 and H3K27ac marks at 24 (data not shown) and 48 hpf (Fig. 2A). A first 7 kb putative element, *hmx1-En1*, was located immediately upstream of the *hmx1* gene, a second 7 kb putative element, *hmx1-En2*, was located more distally and a third 1.8 kb putative element, *hmx1-En3*, was located between the *hmx1* and *hmx4* genes. We tested the enhancer activity of these sequences by generating stable transgenic lines expressing EGFP targeted to the plasma membrane by the CAAX prenylation motif of Ras (Moriyoshi et al., 1996) under the control of each of these elements. Although *hmx1-En3* did not exhibit any enhancer activity, *hmx1-En1* and *hxm1-En2* drove EGFPCAAX expression in specific and partially overlapping regions at 96 hpf. Both enhancers were active in the pharyngeal arches and lips, but only *hmx1-En2* drove EGFP expression in the nasal retina and lens (Fig. 2B-C′). As developmental enhancers can be found in evolutionarily conserved regions (Irimia et al., 2012; Woolfe et al., 2005), we used a multi-species alignment [visualized in the University of California, Santa Cruz (UCSC) genome browser; Kent et al., 2002] to identify conserved domains within *hmx1-En2*. We delineated a 3 kb region, *hmx1-En2s* that was conserved across teleosts and amphibians. However, that region did not exhibit any enhancer activity despite its location within *hmx1-En2*.

As *hmx1-En2* was the only enhancer driving expression in the nasal retina at 96 hpf, we analyzed its activity throughout retinal development in more detail (Fig. 3). At 24 hpf, before RGCs differentiate (Hu and Easter, 1999; Laessing and Stuermer, 1996; Schmitt and Dowling, 1999), EGFP expression was strongly detected in the nasal retina and lens of Tg[*hmx1-En2:EGFPCAAX*] transgenic embryos (Fig. 3A-B′). EGFP remained selectively expressed in the nasal retinal half at 48 (Fig. 3C-D′) and 96 hpf (Fig. 3E-F′). Interestingly, although *hmx1* transcripts were only detected in the RGC layer at 72 and 96 hpf (Fig. 1F,G), EGFP remained visible in the entire nasal retina, likely because of its perdurance *in vivo*. Like *hmx1* transcripts, EGFP was also found in other structures and was

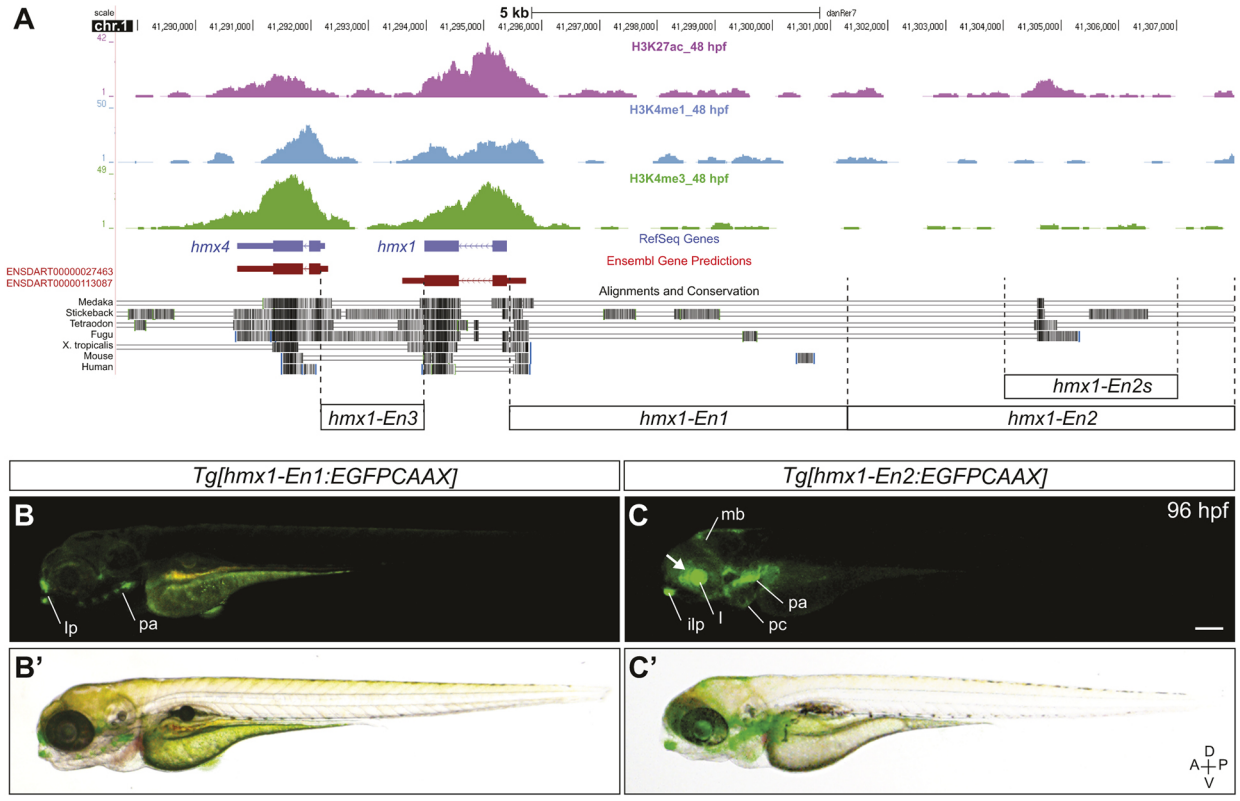

Fig. 2. *Hmx1* enhancers recapitulate *hmx1* endogenous expression. (A) Schematic of the *hmx1*/*hmx4* locus on chromosome 1 (Zv9 assembly, UCSC Genome browser; Kent et al., 2002). The distribution of H3K27ac, H3K4me1, and H3K4me3 modifications at 48 hpf is shown (tracks from Bogdanovic et al., 2012). Four putative regulatory regions named *hmx1-En1*, *hmx1-En2*, *hmx1-En2s* and *hmx1-En3* were tested for enhancer activity in stable transgenic larvae. (B,B′) *Hmx1-En1* drives EGFPCAAX expression in the pharyngeal arches (pa) and lip (lp) region at 96 hpf. (C,C′) *Hmx1-En2* drives expression in the nasal retina (arrow), lens (l), midbrain (mb), pa, inferior lip (ilp) and pericardic (pc) region at 96 hpf. Epifluorescence microscopy, scale bar: 200 µm.

Development (2021) 148, dev199584. doi:10.1242/dev.199584

noticeably detected in the midbrain at 96 hpf (Fig. 3E,E′). To determine whether *hmx1-En2* could drive transgene expression in nasal RGCs, we crossed our Tg[*hmx1-En2:EGFPCAAX*] transgenic line to Tg[*isl2b:TagRFP*] transgenic fish that express TagRFP under the control of the RGC-specific *isl2b* promoter (Pittman et al., 2008; Poulain and Chien, 2013). Confocal analysis of double transgenic larvae at 96 hpf revealed that EGFP partially overlapped with TagRFP in the nasal retina (Fig. 3G-H′). Importantly, we could also detect EGFP in nasal retinal axons innervating the posterior half of the tectum (Fig. 3G,G′), indicating that *hmx1-En2* is effective at driving selective expression in nasal RGCs at late developmental stages.

Hmx1:cre-mediated recombination of an *RGC:colorswitch* reporter enables the visualization of the A/P retinotopic map *in vivo*

As the entire nasal retina and several brain structures beside the tectum were labeled in Tg[*hmx1-En2:EGFPCAAX*] transgenic larvae, we next sought to generate a stable transgenic line that would allow the direct visualization of the A/P retinotectal map *in vivo*. The *Cre/loxP* system has been employed extensively in zebrafish for conditional expression and lineage-tracing analyses (Kawakami, 2007; Mosimann et al., 2011; Yoshikawa et al., 2008). We therefore took advantage of that system to restrict transgene expression to nasal or temporal RGCs. We generated a Tg[*hmx1-En2:cre*] stable transgenic line that expresses *cre* in the nasal retina, and a Tg[*isl2b:loxP-TagRFPCAAX-loxP-EGFPCAAX*] stable reporter line that expresses a switch transgene in RGCs (hereafter referred to as Tg[*RGC:colorswitch*]). To ensure that the *RGC:colorswitch* reporter transgene has integrated in an optimal genomic location for Cre-dependent recombination and to eliminate any functional positional effect, we established three independent Tg[*RGC:colorswitch*] stable lines and tested their responsiveness to Cre by crossing them to Tg[*hsp70l:cre*] transgenic fish. We selected the Tg[*RGC:colorswitch*] reporter line, the progeny of which showed complete change of fluorescence in all RGCs following heat shock at 24 hpf (data not shown). We then crossed that line to generate a Tg[*hmx1-En2:cre; RGC:colorswitch*] double transgenic line (Fig. 4A), and analyzed double transgenic larvae by immunolabeling for EGFP and TagRFP at 4 dpf.

High resolution confocal imaging and 3D-rendering of double transgenic larvae revealed a bi-colored retinotectal map along the A/P axis (Fig. 4; Movie 1). We found that larvae had a bi-colored RGC layer in the retina, with nasal and temporal RGCs expressing EGFP and TagRFP, respectively (Fig. 4B,D-D″). We confirmed by ISH that *tagRFP* was specifically expressed by temporal and not nasal RGCs at 4 dpf (Fig. 4D‴) and later stages (Fig. S2). We then analyzed the projection domains of nasal and temporal retinal axons at the tectum. After elongating together along both branches of the optic tract (Fig. 4C), TagRFP-positive temporal axons terminated in the anterior tectal half (Fig. 4B″,C′), whereas EGFP-positive nasal axons projected through the anterior tectum to reach the posterior tectum (Fig. 4B‴,C″). The sharp boundary between the nasal and temporal projection domains appeared to split the tectal neuropil into two equivalent halves (Fig. 4B,B′,C). Thus, our observations indicate that *hmx1:cre*-mediated recombination can be used to drive selective transgene expression in nasal versus temporal RGCs. Our results also establish the Tg[*hmx1-En2:cre; RGC:colorswitch*] transgenic line as the first genetic model allowing the direct visualization of retinotopic mapping *in vivo* throughout development.

The A/P retinotopic map is established early and remains dynamic

We next examined retinotopic mapping in living larvae from 3 to 6 dpf (Fig. 5) by establishing a consistent imaging and quantification method across larvae for reproducible and unbiased analyses (Fig. S3). Confocal stacks of the retinotectal system were consistently rotated along the *x*, *y*, and *z*-axes to orient all larvae in a similar and comparable manner (Fig. 5A,A′; Fig. S3A,A′). We then

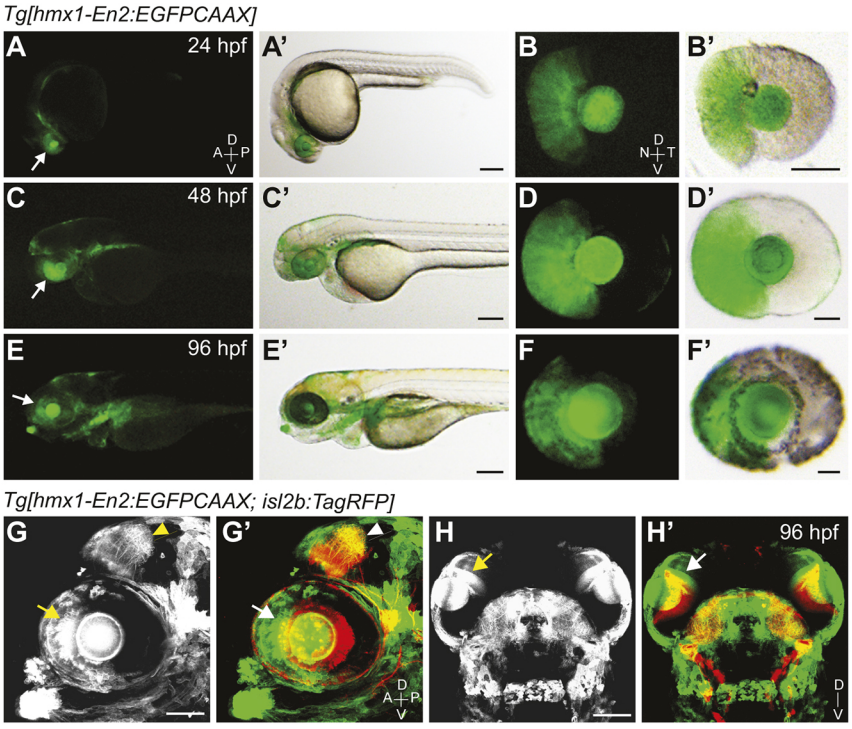

Fig. 3. *Hmx1-En2* drives expression in the nasal retina throughout development. (A-F′) Epifluorescence microscopy (A-F) and corresponding bright-field images (A′-F′) showing EGFPCAAX expression in Tg[*hmx1-En2:EGFPCAAX*] transgenic embryos (A,C,E) and dissected eyes (B,D,F) at 24, 48 and 96 hpf. Fluorescence is detected in the nasal but not temporal retina (arrows) at all stages. (G-H′) Confocal microscopy showing lateral (G,G′) and dorsal (H,H′) views of a double transgenic larvae expressing EGFPCAAX driven by *hmx1-En2* and *TagRFP* in RGCs at 96 hpf. EGFPCAAX is observed in nasal RGCs (arrows) and corresponding axons projecting to the posterior tectum (arrowheads). Scale bars: 200 µm (A,C,E); 50 µm (B,D,F); 100 µm (G,H).

Development (2021) 148, dev199584. doi:10.1242/dev.199584

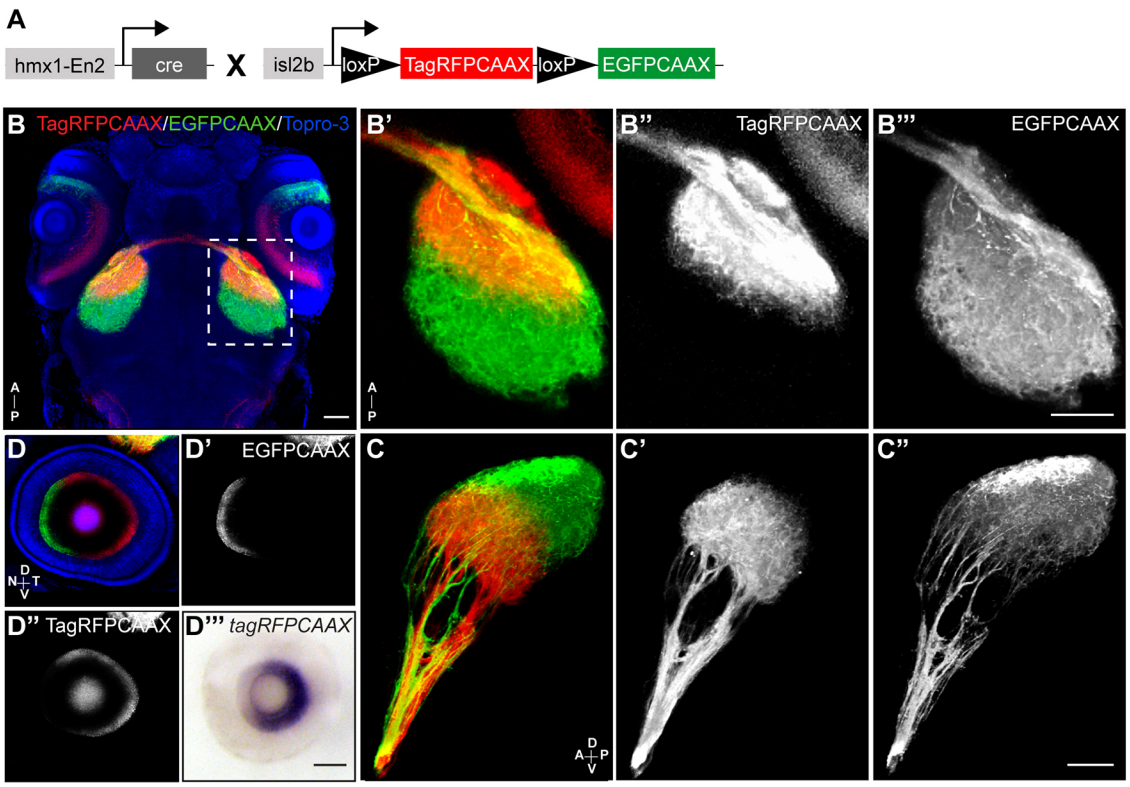

Fig. 4. *Hmx1:cre*-mediated recombination of an *RGC:colorswitch* reporter enables the visualization of the A/P retinotopic map *in vivo*. (A) Schematic of the *hmx1-En2:cre* and *isl2b:loxP-TagRFPCAAX-loxP-EGFPCAAX* (*RGC:colorswitch*) transgenes expressed in double transgenic larvae. (B) Confocal microscopy with 3D rendering showing dorsal view of a transgenic larva immunolabeled for TagRFP and EGFP at 4 dpf. To-Pro-3 was used as a nuclear counterstain to delineate the tectal neuropil. (B′-B‴) TagRFP-positive temporal axons project specifically to the anterior tectal half (B″), whereas EGFP-positive nasal axons project through the anterior to the posterior tectum (B‴). (C-C″) Nasal and temporal axons intermingle in the optic tract but project to distinct tectal halves. (D-D″) EGFP-positive and TagRFP-positive RGCs are restricted to the nasal and temporal retina, respectively. (D‴) Eye of a transgenic larva stained for *tagRFP* by ISH at 4 dpf. *TagRFP* expression remains restricted to the temporal retina. Scale bars: 50 µm (B-D‴).

used maximal projections of rotated stacks to delineate several landmarks at the tectum and analyze the projection domains of nasal and temporal retinal axons (Fig. 5A″; Fig. S3B-B″).

At 3 dpf, when the retinotectal map can first be visualized in fixed embryos (Burrill and Easter, 1995; Stuermer, 1988), we found that EGFP-positive nasal axons had already elongated through the anterior half of the tectum to innervate the posterior half (Fig. 5B). Some nasal axons also seemed to arborize in the anterior tectal half, just rostral to the equator. On the other hand, TagRFP-positive temporal axons projected specifically to the anterior tectum and were not observed in the posterior half (Fig. 5B′). From 4 to 6 dpf, the projection domain of temporal axons expanded within the anterior tectal half, thereby pushing the TagRFP boundary towards the equator (Fig. 5C′-E″). Conversely, the projection domain of EGFP-positive nasal axons appeared denser and progressively more restricted to the posterior tectal half (Fig. 5C-E). To better analyze the dynamics of retinotopic map formation, we quantified the tectal area covered by nasal and temporal axons over time (Fig. 5F-J; Fig. S3B″). Overall, the total tectal coverage (area of the tectum covered by nasal and temporal axons) significantly increased from 3 to 6 dpf (P<0.001), indicating a continuous growth and innervation of the tectum (Fig. 5F). The area covered by temporal axons in the anterior half of tectum steadily and significantly increased as well (Fig. 5G). The arborization field of temporal axons (area covered by temporal axons over the entire tectum) also progressively expanded from 3 to 6 dpf (Fig. 5H), suggesting that the increasing innervation by temporal axons significantly contributes to the tectum growth. Finally, the area covered by EGFP-positive nasal axons in the posterior half of the tectum also steadily and significantly increased from 3 to 5 dpf (P<0.001), but then remained stable from 5 to 6 dpf (Fig. 5I). Thus, our results demonstrate that the A/P retinotopic map is formed early but remains dynamic, with both nasal and temporal projection domains expanding over time.

Nasal projections refine over time and generate a more precise map

In contrast to temporal axons that reach the anterior tectum immediately, nasal retinal axons must navigate through the anterior half of the tectum to reach their correct target in the posterior half. Interestingly, we noticed that some nasal axons appeared to arborize in the anterior tectal half just rostral to the equator at 3 and 4 dpf (Fig. 5B,C). However, these arborizations were not as clearly observed at 5 dpf, as shown by the apparent decrease in EGFP intensity between 4 and 5 dpf (arrows in Fig. 5C,D). We analyzed in more detail the tectal coverage of nasal axons in the anterior half of the tectum. Strikingly, the area covered by nasal axons in the anterior tectum significantly decreased between 3 and 5 dpf but remained stable between 5 and 6 dpf (Fig. 5J). Although the values obtained at 6 dpf likely represent fluorescence from the nasal axonal bundles that have extended through the anterior tectum, the significant decrease in tectal coverage observed from 4 to 5 dpf suggests that nasal retinal projections in the anterior tectal half might refine during that period. We thus calculated a nasal axon mistargeting index (NAMI) as the ratio between the anterior and

Development (2021) 148, dev199584. doi:10.1242/dev.199584

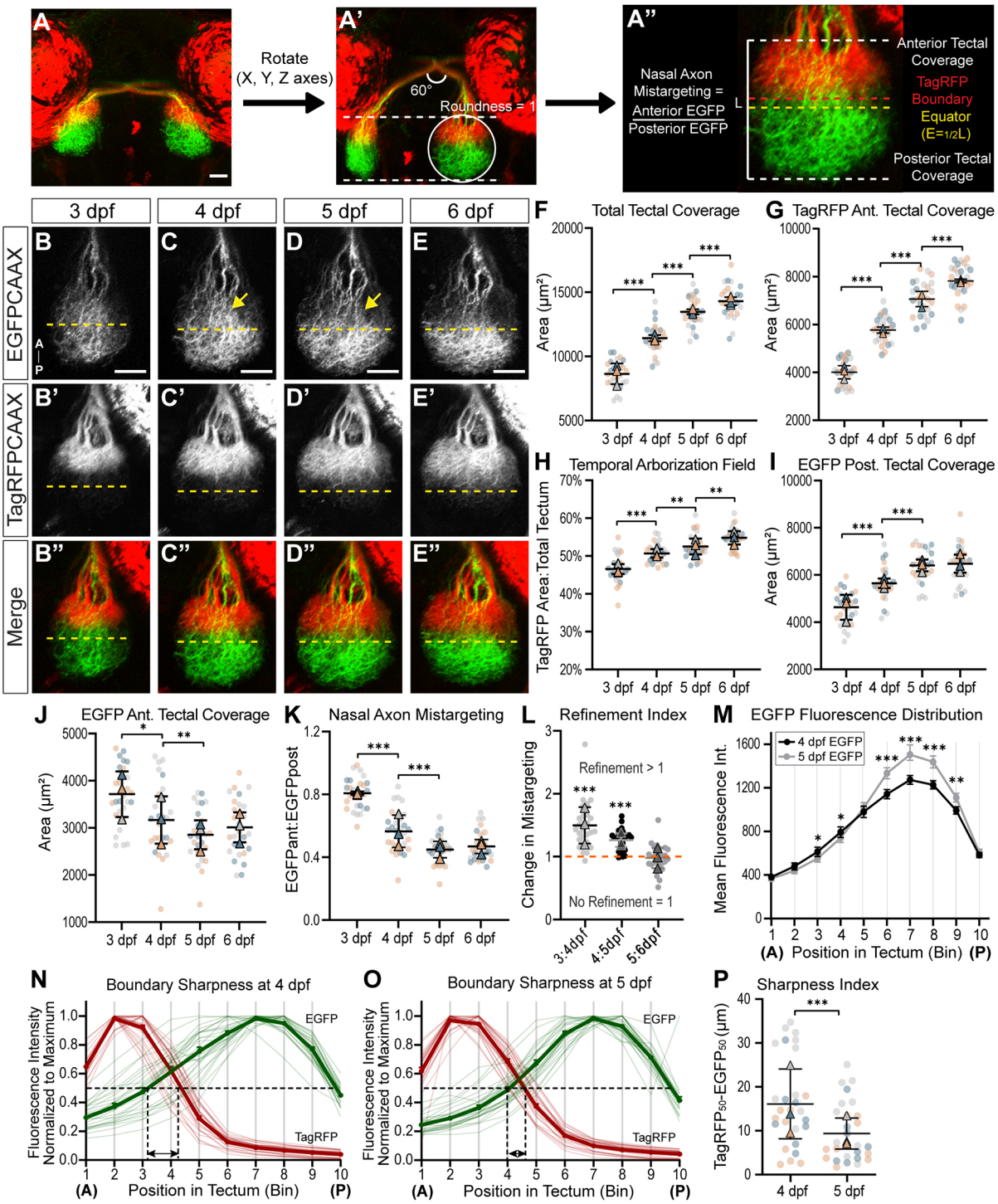

Fig. 5. See next page for legend.

posterior tectal areas covered by nasal axons (Fig. 5K). That index significantly decreased between 3 to 4 dpf and 4 to 5 dpf, but remained stable between 5 and 6 dpf. We also established a refinement index corresponding to the change in the NAMI between two consecutive days (Fig. 5L). The refinement index was greater than 1 between 3 and 4 dpf, and 4 and 5 dpf, indicating a refinement of nasal retinal projections between these stages. That refinement was not due to an absence of Cre recombination in later-born axons, as no *tagRFP* transcripts could be detected in nasal RGCs at 4, 5 or 6 dpf (Fig. S2). In contrast, the refinement index averaged a value of 1 between 5 and 6 dpf (0.97±0.04; mean±s.e.m.), indicating that no detectable refinement occurred over that period. Thus, our results indicate that nasal retinal axons refine and condense their projection domain to the posterior tectum from 3 to 5 dpf.

To determine the effect of that refinement on the retinotopic map, we decided to analyze the sharpness of the map at 4 and 5 dpf. We used sum projections of rotated stacks to measure the mean fluorescence intensity of EGFP and TagRFP in bins of equal height distributed along the A/P axis of the tectum (Fig. S3C-C″). Interestingly, the mean EGFP intensity significantly decreased

Development (2021) 148, dev199584. doi:10.1242/dev.199584

Fig. 5. Nasal axons refine their tectal projection domain between 4 and 5 dpf. (A-A″) Summarized quantification method to analyze retinotopic mapping (see details in Fig. S3). (A″) The anterior tectal boundary was defined as the rostral limit of the tectum (white dashed line), the posterior boundary, as the caudal end of the tectum (white dashed line), the TagRFP boundary (red dashed line) as the caudal limit of the TagRFP signal, and the equator (E; yellow dashed line) as half of the total tectum length (L) measured between the rostral and caudal tectal boundaries. The tectal area rostral to the equator was defined as the anterior tectal half, the area caudal to the equator as the posterior half. (B-E″) Confocal microscopy showing the development of the A/P retinotopic map from 3 to 6 dpf. (B-E) EGFP-positive nasal axons progressively refine their targeting domain to the posterior tectal half. Axons mistargeting the anterior tectal half appear to disappear between 4 and 5 dpf (arrows). (B′-E′) TagRFP-positive temporal axons target the anterior tectal half. (B″-E″) The A/P topographic map is established early and maintained as retinal axons continue to innervate the tectum. The temporal retinal arborization field expands to fill the anterior tectal half, reaching the equator position by 6 dpf. (F) The total tectal area covered by TagRFP-positive and EGFP-positive axons significantly increases from 3 to 6 dpf. (G) The anterior area of the tectum covered by temporal axons also steadily increases from 3 dpf and 6 dpf. (H) The temporal arborization field, defined as the ratio of the TagRFP area of coverage to the total tectal area, progressively expands from 3 to 6 dpf. (I) EGFP-positive nasal axons terminating in the posterior tectal half cover a significantly larger area between 3 and 4 dpf, and 4 and 5 dpf, before the area of coverage stabilizes between 5 and 6 dpf. (J) The anterior tectal area covered by EGFP nasal axons significantly decreases between 4 and 5 dpf, indicating a refinement of the nasal projection domain. (K) The nasal axon mistargeting index (NAMI), defined as the ratio between the anterior and posterior tectal areas covered by EGFP-positive nasal axons, significantly decreases between 3 and 4 dpf as well as between 4 and 5 dpf. (L) The refinement index corresponding to the change in the NAMI between two consecutive days is greater than 1 between 3 and 4 dpf, and 4 and 5 dpf, indicating a refinement of nasal projections. It averages a value of 1 between 5 and 6 dpf, indicating no refinement during that period. (M) The mean EGFP fluorescence intensity was measured in 10 bins distributed along the A/P axis of the tectum at 4 and 5 dpf. It significantly decreases in anterior bins 3 and 4 from 4 to 5 dpf while increasing in posterior bins 6-9. (N,O) Normalized fluorescence intensities of EGFP and TagRFP were plotted along the A/P axis of the tectum. The distance from the anterior tectal boundary at which EGFP and TagRFP intensities reached 50% of their maximal value is marked by dashed lines. It decreases between 4 and 5 dpf (double arrows), indicating a sharpening of the boundary between EGFP and TagRFP projection domains. (P) The boundary sharpness index corresponding to the distance between $EGFP_{50\%}$ and $TagRFP_{50\%}$ (double arrows in N and O) significantly decreases between 4 and 5 dpf. Data are mean±s.e.m. **P*<0.05, ***P*<0.01, ****P*<0.001 [one-way ANOVA with Tukey's multiple comparisons post-hoc test (F-K); two-tailed, paired *t*-test (L,M,P)]. *n*=27 larvae. Circles represent individual larvae; triangles represent mean. Scale bars: 50 µm.

between 4 and 5 dpf in anterior bins 3 and 4, whereas it significantly increased in posterior bins 6-9 (Fig. 5M). We further analyzed the sharpness of the EGFP-TagRFP boundary by normalizing fluorescence intensities to their maximum values at 4 and 5 dpf and plotting them along the A/P axis (Fig. 5N,O). We then determined the distance from the anterior tectal boundary at which EGFP and TagRFP intensities reached 50% of their maximal value (dashed lines in Fig. 5N,O). Interestingly, $EGFP_{50\%}$ shifted from an averaged position of 40.73±13.16 µm at 4 dpf (anterior region of bin 3) to 53.45±9.92 µm (bin 4) at 5 dpf. In contrast, $TagRFP_{50\%}$ kept a similar location between bins 4 and 5 from 4 to 5 dpf. We next calculated a sharpness index corresponding to the absolute value of the distance between $EGFP_{50\%}$ and $TagRFP_{50\%}$ (double arrows in Fig. 5N,O). That index significantly decreased between 4 and 5 dpf (Fig. 5P), demonstrating that the boundary between nasal and temporal projection domains sharpens during that interval. Thus, our results demonstrate that the zebrafish retinotectal map sharpens and becomes more precise as nasal projections refine and disappear from the anterior tectum.

Cntn2 is required for refining nasal projections and sharpening the retinotectal map

Our unique ability to analyze subtle dynamic changes in retinotopic mapping over time prompted us to test whether we could use our transgenic line to discover as yet unreported gene functions. Cntn2 is an adhesion molecule known to promote axon growth and fasciculation in several brain circuits (Mohebiany et al., 2014). It has been specifically detected in the nasal retina in zebrafish (Gurung et al., 2018; Lang et al., 2001; Warren et al., 1999), but its role in the retinotectal system has remained surprisingly uncharacterized. We therefore decided to test whether Cntn2 could regulate retinotectal mapping along the A/P axis. We first confirmed that *cntn2* was strongly and selectively expressed in the nasal RGC layer from 3 to 6 dpf (Fig. 6A-B), suggesting it might regulate the targeting and/or maturation of nasal projections at the tectum. We then took advantage of the two-RNA component (crRNA:tracrRNA) version of the CRISPR system (Jacobi et al., 2017) to induce *cntn2* mutations in transgenic embryos. We designed two independent crRNAs targeting sequences in exons 3 and 5 that encode the first and second N-terminal Ig-like domains of Cntn2, respectively. As previously described (Hoshijima et al., 2019), crRNA:tracrRNA:Cas9 ribonucleoprotein (RNP) complexes were highly effective at inducing mutations directly in injected 'crispant' embryos (Fig. S4). Crispant larvae injected with either RNP complex (gRNA1 or gRNA2) or a combination of both gRNAs were undistinguishable from Cas9-injected controls and did not exhibit any obvious morphological or developmental defects.

We then analyzed retinotopic mapping in *cntn2* crispants at 4 and 5 dpf. Both crispants and controls had a bi-colored A/P retinotectal map at both stages (Fig. 6A-F′), with nasal axons innervating the posterior tectal half and temporal axons, the anterior half. Quantifications showed a similar increase in the total tectal coverage from 4 to 5 dpf in crispants and controls, indicating a normal tectal growth (Fig. 6G). We did not observe any difference in the temporal arborization field between crispants and controls (Fig. 6I), and the anterior tectal coverage of temporal axons increased similarly among groups from 4 to 5 dpf (Fig. 6H), suggesting that *cntn2* mutations did not overly affect temporal projections. We noticed, however, that nasal projections did not appear to disappear from the anterior tectum at 5 dpf in crispants (Fig. 6C,D) compared with controls (Fig. 6E,F). Although the posterior tectal coverage of nasal axons increased in both crispants and controls (Fig. 6J), we observed significant differences in the anterior tectal coverage, which decreased in controls but remained constant or slightly increased in *cntn2* crispants (Fig. 6K). Likewise, the NAMI significantly decreased in controls but not in crispants (Fig. 6L), demonstrating that the refinement of nasal projections does not occur when *cntn2* is mutated. Interestingly, both anterior tectal coverage and NAMI remained remarkably constant from 5 to 6 dpf in crispants, further indicating that the nasal projection domain does not refine even at a later stage in the absence of Cntn2 (Fig. S5B,C). Lack of refinement was further confirmed by the refinement index that averaged 1 from 4 to 6 dpf in crispants (Fig. 6N; Fig. S5D). As the refinement of nasal projections correlates with a sharpening of the retinotopic map (Fig. 5), we next examined how the refinement defects observed in *cntn2* crispants might affect topographic mapping. Analysis of the EGFP-TagRFP boundary sharpness at 4 and 5 dpf revealed that the distance between $EGFP_{50\%}$ and $TagRFP_{50\%}$ did not decrease in crispants compared with controls (Fig. S6). Moreover, the sharpness index remained stable in crispants instead of decreasing like in controls (Fig. 6M), demonstrating that *cntn2* is necessary for retinotectal map sharpening. As *cntn2* is known to modulate

Development (2021) 148, dev199584. doi:10.1242/dev.199584

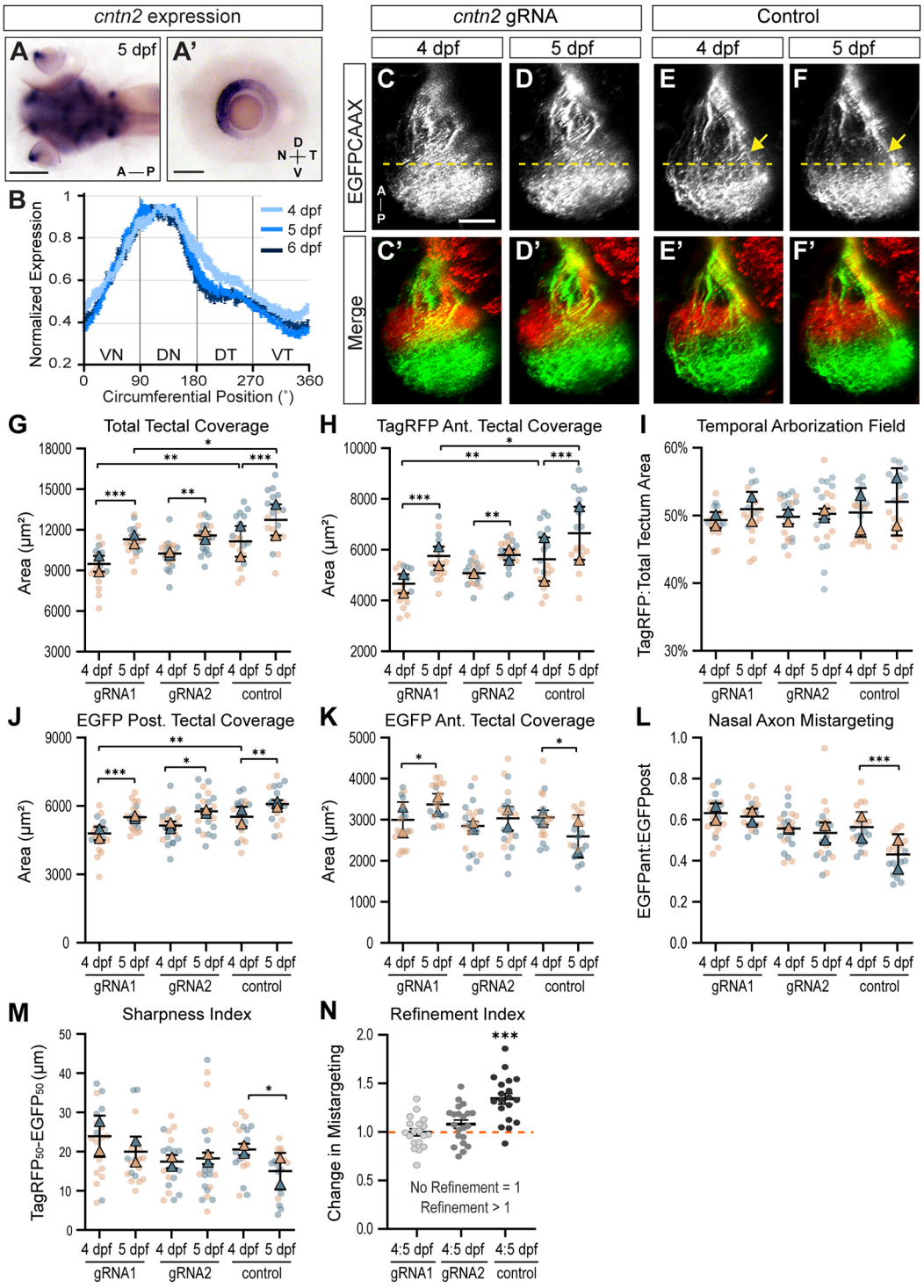

Fig. 6. Cntn2 is required for the refinement of nasal projections and map sharpening. (A,A′) Larva and dissected eye stained for *cntn2* by ISH at 5 dpf. *Cntn2* is strongly expressed in the nasal RGC layer. (B) *Cntn2* expression is restricted to the nasal RGC layer at 4, 5 and 6 dpf. (C-F′) Confocal microscopy showing the development of the A/P retinotopic map in *cntn2* gRNA-injected larvae (C-D′) and Cas9-injected control larvae (E-F′) from 4 to 5 dpf. The anterior tectal area covered by EGFP-positive nasal axons does not change between 4 and 5 dpf in *cntn2* crispants, whereas it appears to decrease in control larvae (E-F, arrows). (G) The total tectal area significantly increases in crispants injected with gRNA1 or gRNA2 and in control larvae between 4 and 5 dpf. (H) The anterior area of the tectum covered by temporal axons significantly increases between 4 and 5 dpf in both crispants and controls. (I) The temporal arborization field is similar between *cntn2* crispants and controls. (J) The area covered by nasal axons in the posterior half of the tectum significantly increases in *cntn2* crispants and controls. (K) The area covered by nasal axons in the anterior tectal half significantly decreases between 4 and 5 dpf in controls but not in crispants, indicating an absence of refinement in crispants. (L) The nasal axon mistargeting index decreases in controls but remains unchanged in crispants. (M) The boundary sharpness index remains constant in *cntn2* crispants, indicating that the boundary between EGFP and TagRFP projection domains does not refine over time (see also Fig. S5). (N) The refinement index is greater than 1 in controls but averages 1 in crispants, confirming the absence of refinement of the nasal projection domain. Data are mean±s.e.m. **P*<0.05, ***P*<0.01, ****P*<0.001 (mixed effects one-way ANOVA followed by Tukey's multiple comparisons post-hoc test). *n*=19 gRNA1 crispants, 21 gRNA2 crispants, 19 controls. Circles represent individual larvae; triangles represent mean. Scale bars: 100 µm (A); 50 µm (A′,C-F′).

Development (2021) 148, dev199584. doi:10.1242/dev.199584

neurogenesis at early stages of nervous system development (Ma et al., 2008), we next tested whether the loss of *cntn2* could affect retinal patterning along the A/P axis. Analysis and quantification of *hmx1* expression throughout retinotectal development revealed a normal retinal patterning in *cntn2* crispants (Fig. S7), indicating that the absence of tectal refinement is not due to a loss of RGC positional identity in the retina. Thus, by detecting subtle retinotectal targeting phenotypes in *cntn2* crispants, our study unraveled a novel function for Cntn2 in refining and sharpening retinal projections during visual system maturation.

DISCUSSION

Our understanding of topographic map development and maturation has so far been limited by a lack of genetic models allowing the direct observation of maps over time. Here, we report the generation of a novel zebrafish transgenic line that, for the first time, enables the unbiased and quantitative analysis of retinotopic map formation and refinement directly *in vivo*. Using live confocal imaging of transgenic larvae from 3 to 6 dpf, we show that the A/P retinotopic map is formed at early stages but remains dynamic as both retina and tectum grow, with the projection domains of nasal and temporal axons expanding over time. We further demonstrate that nasal retinal projections initially arborize in the anterior tectal half but progressively refine and condense their projection domain to the posterior tectum from 4 to 5 dpf, leading to the sharpening of the A/P retinotopic map. Finally, we demonstrate that Cntn2, an adhesion molecule expressed in nasal RGCs, is required for the refinement of nasal retinal axons and retinotectal map sharpening.

In agreement with previous studies in zebrafish and other species (Boisset and Schorderet, 2012; Deitcher et al., 1994; Schulte and Cepko, 2000; Stadler and Solursh, 1994; Wang et al., 2000; Yoshiura et al., 1998), our data reveal that the homeobox transcription factors *hmx1* and *hmx4* are expressed in a sharp nasal-high to temporal-low gradient in the retina throughout development. The detection of *hmx1* and *hmx4* throughout the nasal retinal neuroepithelium at early stages indicates that both genes are expressed in proliferating neuroblasts and might regulate their positional identity and differentiation. Supporting that hypothesis, reduced *hmx1* expression has been shown to block retinal cell differentiation in zebrafish (Boisset and Schorderet, 2012; Schorderet et al., 2008) and cause microphthalmia in mouse (Munroe et al., 2009) and human (Gillespie et al., 2015; Schorderet et al., 2008; Vaclavik et al., 2011). Although zebrafish embryos lacking functional *hmx1* do not exhibit any eye patterning defect (Boisset and Schorderet, 2012), misexpression of *hmx1* or *hmx4* does alter the regional specification of the retina along the nasal-temporal axis in chick (Schulte and Cepko, 2000; Takahashi et al., 2009), suggesting that *hmx1* and *hmx4* have redundant functions in teleosts. Interestingly, our analysis shows that the expression of both *hmx1* and *hmx4* becomes restricted to the nasal RGC and inner nuclear layers at later stages. We have also identified a distal regulatory element upstream of *hmx1* and *hmx4* genes that drives expression in nasal RGCs at 4 dpf and later. Altogether, these data suggest that *hmx1* and *hmx4* are expressed by mature RGCs themselves at late stages of development. Supporting that observation, *hmx1* transcripts have been detected in RGCs, horizontal cells and Müller glia of the adult human retina by single cell profiling (Cowan et al., 2020; Lukowski et al., 2019; Voigt et al., 2019). Examining the effects of manipulating *hmx1* expression in nasal or temporal RGCs will thus be of great interest to better understand the progression of the oculoauricular syndrome caused by *hmx1* mutations in human (Gillespie et al., 2015; Schorderet et al., 2008; Vaclavik et al., 2011).

Using *hmx1:cre*-mediated recombination of an *RGC:colorswitch* reporter, we have generated a novel transgenic line that enables the unprecedented visualization of the A/P retinotopic map *in vivo*. We were able to image and analyze for the first time retinotectal map development within the same larvae over successive days. This unparalleled temporal resolution allowed us to observe dynamic changes in retinotopic mapping that could not be seen previously in fixed embryos. We found that, although the A/P retinotopic map is established early on, it progressively shifts caudally as temporal axons expand their innervation of the anterior tectum. This caudal shift is accompanied by the progressive refinement of nasal projections that condense their projection domain to the posterior tectum. Interestingly, the parameters of retinotopic mapping we measured did not show much variability across larvae, indicating that retinotopic mapping is a robust and highly stereotyped process. That property allowed us to characterize in detail the dynamic changes underlying retinotopic map maturation. Notably, we found that nasal projections initially covering the caudal part of the anterior tectum refine and progressively condense their domain to the posterior half between 3 and 5 dpf. This refinement is unlikely to be caused by cell death in the retina, as apoptosis in the RGC layer peaks from 1.5 to 3 dpf before sharply decreasing from 4 to 6 dpf (Biehlmaier et al., 2001; Cole and Ross, 2001). Instead, it is likely driven by the dynamic rearrangement of axonal branching pattern as nasal axons extend caudally and arborize in their final zone in the posterior tectum. In *Xenopus*, nasal axons retract their branches from the anterior tectum after initiating branches in both anterior and posterior tectal halves (O'Rourke and Fraser, 1990). Although retinal axons in zebrafish were initially thought to elongate along straight trajectories and only arborize after reaching their target area (Kaethner and Stuermer, 1992), more recent studies using high-resolution time-lapse imaging have instead revealed that axons continuously extend and retract branches and navigate by selective branch stabilization (Kita et al., 2015; Simpson et al., 2013). Once in their termination area, axonal arbors remain highly dynamic, with only a small fraction of them being maintained in the mature arbor (Alsina et al., 2001; Ben Fredj et al., 2010; Campbell et al., 2007; Meyer and Smith, 2006; Munz et al., 2014; Ruthazer et al., 2006). A retraction of proximal branches that have extended in inappropriate areas coupled with a constant remodeling of arborizing axons might thus redistribute the position of branches and cause arbors to shift caudally, leading to the progressive refinement of nasal projections we observed.

Using a CRISPR-mediated functional approach in our retinotopic transgenic line, we found that the refinement of nasal projections requires Cntn2, a glycosylphosphatidylinositol (GPI)-anchored adhesion molecule selectively expressed in the nasal retina throughout development. Although previous studies had described the selective expression of *cntn2* in the nasal retina in zebrafish (Gurung et al., 2018; Lang et al., 2001; Warren et al., 1999), none had reported a function for Cntn2 in retinotopic mapping, likely because the labeling methods available then did not allow for the visualization of nasal projections refining over time in a living animal. Our detection and unbiased analysis of retinotectal maturation *in vivo* revealed that retinotopic map sharpening is prevented in *cntn2* crispants, indicating that the remodeling of nasal retinal projections strongly contributes to the increasing precision of the retinotopic map. Interestingly, we did not observe any defects in the initial tectal coverage of nasal or temporal axons in *cntn2* crispants, suggesting that retinal axon elongation and guidance

Development (2021) 148, dev199584. doi:10.1242/dev.199584

are not affected in the absence of Cntn2. The lack of an earlier phenotype is unlikely to be caused by an incomplete knockdown, as we did not detect any additional phenotypes or worsened refinement defects in crispants injected with a combination of gRNAs (Fig. S8). Our results rather highlight a specific, later role for Cntn2 in the visual system that contrasts with its known functions at earlier developmental stages in other circuits (Masuda, 2017). Indeed, Cntn2 is known to regulate axon growth, guidance and fasciculation in several systems (Mohebiany et al., 2014). It is required for the proper guidance of spinal commissural axons and cerebellar granule cell axons in chick (Baeriswyl and Stoeckli, 2008; Fitzli et al., 2000; Stoeckli and Landmesser, 1995). In mice, it regulates the fasciculation of dorsal root ganglion (DRG) axons (Law et al., 2008) and controls the guidance and fasciculation of motor axons, preventing them from entering DRGs (Suter et al., 2020). In zebrafish, Cntn2 promotes the growth and fasciculation of axons extending from the nucleus of the medial longitudinal fascicle (Gurung et al., 2018; Wolman et al., 2008). Cntn2 is the only member of the contactin family known to participate in homophilic interactions (Mohebiany et al., 2014). It also engages in heterophilic interactions with other adhesion molecules (Buchstaller et al., 1996; Fitzli et al., 2000; Kuhn et al., 1991; Kunz et al., 1998; Suter et al., 1995), raising the possibility that the lack of refinement observed in *cntn2* crispants might result from a fasciculation defect among nasal axons that would delay nasal axon extension to the posterior tectum. However, we did not observe any fasciculation defects of nasal axons as they navigate along the optic chiasm and optic tract. The lack of tectal refinement persisting at late stages in *cntn2* crispants also argues against a delayed phenotype. Instead, Cntn2 might regulate the selective retraction of proximal nasal axonal branches that have inappropriately extended in the anterior tectum. Cntn2 might, for example, modulate the responsiveness of axonal branches to a repellant cue enriched in the anterior tectal region, just as it regulates the sensitivity of sensory axons to semaphorins (Law et al., 2008; Dang et al., 2012).

Alternatively, Cntn2 might promote retinotectal refinement by modulating the activity of RGCs. Spatiotemporal patterns of retinal activity are indeed known to drive the sharpening of visual circuits in vertebrates (Burbridge et al., 2014; Cang et al., 2005; Chandrasekaran et al., 2005; Dhande et al., 2011; Hiramoto and Cline, 2014; Munz et al., 2014; Rahman et al., 2020; Ruthazer et al., 2003; Stellwagen and Shatz, 2002; Xu et al., 2015, 2016; Zhang et al., 2011). Activity is notably required for the elimination of branches with a firing pattern that does not match that of their neighbors. Consequently, blocking neuronal activity with tetrodotoxin causes enlarged axonal arbors in frog (Cohen-Cory, 1999; Reh and Constantine-Paton, 1985) and prevents the refinement of retinal fibers that overshoot their termination zone in chick (Kobayashi et al., 1990). Similarly in mouse, axons occupy a larger area in the SC after RGCs have been silenced (Benjumeda et al., 2013). In zebrafish, altering RGC activity also modifies the size and morphology of terminal arbors (Ben Fredj et al., 2010; Gnuegge et al., 2001; Hua et al., 2005; Kaethner and Stuermer, 1994; Schmidt et al., 2000; Smear et al., 2007; Stuermer et al., 1990), and the projection field of silenced retinal axons appears to be more diffuse (Ben Fredj et al., 2010; Gnuegge et al., 2001). Interestingly, we observed a lack of nasal axon refinement and map sharpening between 4 and 5 dpf in zebrafish *maco* mutants (Spead and Poulain, 2020b preprint), in which a downregulation of voltage-gated sodium channels causes a lack of neural activity in RGCs and peripheral sensory neurons (Gnuegge et al., 2001; Granato et al., 1996; Ribera and Nüsslein-Volhard, 1998). *Maco* mutants harbor a mutation in *pigk*, a component of the transamidase complex responsible for GPI anchor synthesis and attachment to nascent proteins (Carmean et al., 2015; Ohishi et al., 2000). Although it remains unknown which GPI-anchored proteins are impaired in *maco*, Cntn2 appears as a good candidate considering the shared phenotype between *maco* mutants and *cntn2* crispants. Moreover, Cntn1, another member of the contactin family, is known to interact with several voltage-gated sodium channels via its fibronectin type III-like (Fn-III) domains and to increase their density at the plasma membrane (Chen et al., 2004; Kazarinova-Noyes et al., 2001; Liu et al., 2001; McEwen and Isom, 2004; McEwen et al., 2004; Rush et al., 2005; Shah et al., 2004). Considering the high conservation between the Fn-III domains of Cntn1 and Cntn2, Cntn2 might be able to interact with sodium channels as well. An absence of functional Cntn2 would then alter the distribution of sodium channels in nasal retinal axons, leading to a lack of activity-dependent refinement and map sharpening at the tectum. Conversely, neuronal activity might regulate the targeting of Cntn2 to the plasma membrane, just as it modulates that of Cntn1 in hypothalamic axons (Pierre et al., 2001). Cntn2 would then act downstream of neuronal activity for mediating activity-dependent morphological remodeling. By enabling the visualization of map sharpening over time as well as the selective manipulation of nasal and temporal RGCs, our new genetic model will provide new strategies for analyzing the molecular mechanisms by which Cntn2 and activity cooperate for precise retinotopic mapping *in vivo*.

MATERIALS AND METHODS

Zebrafish husbandry and maintenance

All experiments and procedures were approved by the Institutional Animal Care and Use Committee of the University of South Carolina. Zebrafish wild-type (WT) and transgenic embryos were obtained from natural matings, raised at 28.5°C in E3 medium (5 mM NaCl, 0.17 mM KCl, 0.33 mM $CaCl_2$ and 0.33 mM $MgSO_4$) in the presence of 150 mM of 1-phenyl-2-thiourea (PTU; Millipore Sigma) to prevent pigment formation, and staged by age and morphology (Kimmel et al., 1995). WT embryos were from the Tübingen or AB strains. Embryos were anesthetized in tricaine-S (Western Chemicals) before fixation or imaging. Zebrafish larvae and young fish were nurtured using rotifer suspension and dry food (Gemma 75 and 150, Skretting USA). Adult fish were fed with dry food (Gemma 300, Skretting USA).

Cloning of cDNAs and putative enhancers

For cloning *hmx1*, *hmx4* and *cntn2* cDNAs, zebrafish mRNA was isolated from embryos at 24, 48 and 96 hpf using Trizol and the RNeasy mini kit (Qiagen), and cDNA was prepared from RNA using the SuperScript III First-Strand Synthesis system (Invitrogen). *Hmx1*, *hmx4* and *cntn2* cDNAs were amplified using the following full length primers: *hmx1-fw*, 5′-ATGCATGAAAAAAGCCAGCAACAGC-3′; *hmx1-rv*. 5′-TCAGA-CAAGGCCTGTCATCTGC-3′; *hmx4-fw*, 5′-ATCTAACGGAGAATATG-AGCAAGGAG-3′; *hmx4-rv*, 5′-TCATATATCTCCATCAAACAGGCT-GAAATAC-3′; *cntn2-fw*, 5′-ATGAGGATTCTGTTGTGTCTG-3′; *cntn2-rv*, 5′-TCACAGTCCTGATGAGCCAA-3′. Amplicons were subcloned into PCRII-TOPO (Invitrogen) and sequenced to verify gene identity and confirm sequence orientation (sequencing by Eton Bioscience).

Hmx1 putative enhancer elements were amplified by PCR from total genomic DNA using the LA Taq PCR kit v2.1 (TaKaRa) and the following primers: *hmx1-En1-fw*, 5′-ACCGCACCACTAAAGAGTCACAG-3′; *hmx1-En1-rv*, 5′-GGGTGATACGTGAATACCTCTAAGCA-3′; *hmx1-En2-fw*, 5′-GAGGGTGCCAGATGGAGATACAC-3′; *hmx1-En2-rv*, 5′-ACTGGCTCTGCTATGCTTCTGTTTC-3′; *hmx1-En2s-fw*, 5′-GAACG-GTACCGAACCGTCTATTAAAAGATTACACTAC-3′ (KpnI restriction site added in primer); *hmx1-En2s-rv*, 5′-GAACGGATCCAATAAA-CAAGGGACTAATAATTCAAGG-3′ (BamHI restriction site added in

Development (2021) 148, dev199584. doi:10.1242/dev.199584

primer); *hmx1-En3-fw*, 5′-GAACGGTACCTCTTTGGAGACTGGCT-GAACTGAC-3′ (KpnI restriction site added in primer); *hmx1-En3-rv*, 5′-GAACGGATCCATTCTCCGTTAGATGCGGGTCC-3′ (BamHI restriction site added in primer). Amplicons were purified on gel using the Qiaquick gel extraction kit (Qiagen), subcloned into PCRII-TOPO (Invitrogen) and sequenced before being digested and ligated into the Gateway *p5E-MCS* entry vector (Kwan et al., 2007) using the following restriction endonucleases: XhoI/BamHI (for *hmx1-En1*), DraII (for *hmx1-En2*) and KpnI/BamHI (for *hmx1-En2s* and *hmx1-En3*).

Generation of transgenesis vectors

All transgenesis constructs were generated using the Tol2kit Gateway cloning system (Kwan et al., 2007). To generate *hmx1* reporter constructs, *p5E-hmx1-En1*, *p5E-hmx1-En2*, *p5E-hmx1-En2s*, *p5E-hmx1-En3*, *pME-EGFPCAAX* and *p3E-polyAv2* were recombined into the *pDestTol2pA2* destination vector using a Gateway Multisite LR reaction (Kwan et al., 2007; Invitrogen). *p5E-hmx1-En2*, *pME-iCre* and *p3E-polyAv2* were recombined into *pDestTol2CR3* (*pDestTol2pA3* with *myl7:TagRFP* transgenesis marker) to generate the *hmx1-En2:iCre* construct. The sequence encoding *loxP-TagRFPCAAX-polyA-loxP* was amplified by PCR, purified on gel using the Qiaquick gel extraction kit (Qiagen) and recombined into the pDONR221 destination vector to generate the *pME-loxP-TagRFPCAAX-polyA-loxP* entry vector. A modified *p5E-isl2b-gata2a* entry clone encoding a 7.6 kb genomic fragment upstream of the *isl2b* start codon fused to the 1 kb promoter of *gata2a* (Ben Fredj et al., 2010; Pittman et al., 2008), *pME-loxP-TagRFPCAAX-polyA-loxP*, and *p3E-EGFPCAAX-polyA* were recombined into the *pDestTol2pA2* destination vector to generate the *isl2b:loxP-TagRFPCAAX-loxP-EGFPCAAX* (*RGC:colorswitch*) reporter construct.

Generation of stable transgenic lines

Stable transgenic lines were generated using the Tol2 transposon method as described previously (Kawakami et al., 2000). We co-injected 10 to 40 pg of purified DNA (*pTol2pA2-hmx1-En1:EGFPCAAX, pTol2pA2-hmx1-En2:EGFPCAAX, pTol2pCR3-hmx1-En2:iCre, RGC:colorswitch*) with 25 pg of synthetic mRNA encoding Tol2 transposase at the one-cell stage, and injected embryos with transient expression of transgenes were raised up to adulthood as F0 generation. F0 fish were then out-crossed to WT to screen for positive F1 embryos expressing the transgenes. Expression of TagRFP driven in the heart by the *myl7* promoter was used to identify *hmx1-En2:iCre* carriers. Transgenic F1 carriers were subsequently out-crossed to WT to generate stable lines with a single-copy insertion.

gRNAs target site design and preparation of gRNA:Cas9 ribonucleoprotein complexes

Potential gRNA target sites were identified using the proprietary Alt-R® CRISPR-Cas9 guide RNA design platform developed by Integrated DNA Technologies (IDT). Two independent target sequences in two different exons were chosen based on the high predicted editing performance score (above 65) of the corresponding gRNA and the lack of potential off-target sites with fewer than 2 bp mismatches in the GRCz11 genome. The *cntn2* target sequences (with PAMs in brackets) used in this study were: *cntn2* gRNA1, TGAAGAGTCGCACTACACAC[AGG] (targeting exon 4 of ENSDART00000000486.9 Ensembl transcript); and *cntn2* gRNA2, GGAACTCGTTGATAAACCAG[CGG] (targeting exon 6). Target-specific Alt-R® crRNA and universal Alt-R® tracrRNA were synthesized by IDT. Each RNA was dissolved in nuclease-free duplex buffer (IDT) as a 100 mM stock solution that was stored at −80°C. To prepare the crRNA:tracrRNA duplex, equal volumes of 100 mM Alt-R® crRNA and tracrRNA stock solutions were mixed together, heated for 5 min at 95°C and annealed by gradual cooling at room temperature. Cas9 protein (Alt-R® S.p. Cas9 nuclease V3, IDT) was diluted to 1 µg/µl in 30 mM HEPES (pH 7.5), 100 mM potassium acetate, aliquoted and stored at −20°C. CrRNA:tracrRNA:Cas9 ribonucleoprotein (RNP) complexes were assembled by gently mixing 3 µl of crRNA:tracrRNA duplex and 3 µl of Cas9 stock protein. The RNP solution was heated for 10 min at 37°C and allowed to cool at room temperature. Then 1 µl of 0.25% phenol red solution was added to the RNP complex solution before microinjection. Approximately 2 nl of 5 µM RNP complex solution was injected into the cytoplasm of one-cell-stage embryos. Control embryos were injected similarly with Cas9 only.

Analysis of CRISPR efficiency and detection of *cntn2* mutations

After final imaging of the retinotectal map, genomic DNA was extracted from Cas9 control and *cntn2* gRNA-injected larvae for analyzing gRNA efficiency. Individual larvae were incubated in 20 µl of 50 mM NaOH at 95°C for 25 min. After cooling to 4°C, 2 µl of 1 M Tris-HCl (pH 8.0) was added for neutralization. The presence of mutations at the target sites in exons 4 and 6 was assessed by HRMA in all larvae analyzed, as previously described (Dahlem et al., 2012; Parant et al., 2009). Amplicons including the entire genomic target site were generated using the following primers: *gRNA1-HRMA-fw*, 5′-ATGGCACTGACATAT-CATTTG-3′; *gRNA1-HRMA-rv*, 5′-CCATTCTGAGGGTTGTTGA-3′; *gRNA2-HRMA-fw*, 5′-CTGTTTGTTAGCTTTGTCCTAC-3′; *gRNA2-HRMA-rv*, 5′-GAAACAAACCACCTGCCC-3′. To confirm HRMA results, larger genomic sequences including the target sites were amplified from a subset of larvae and analyzed by sequencing. Amplicons to be sequenced were generated using the following primers: *gRNA1-seq-fw*, 5′-GTGTGTGATTTCCTCCCAG-3′; *gRNA1-seq-rv*, 5′-CCGAACTTGA-GATTAGCGAC-3′; *gRNA2-seq-fw*, 5′-GAACATTTCTTGCCTGCCAG-3′; *gRNA2-seq-rv*, 5′-GCTGAAGATGCTCTTGGTGC-3′.

Whole-mount *in situ* hybridization

For making ISH probes, cDNA templates cloned into pCRII-TOPO were amplified by PCR using M13fw and M13rv primers and purified on gel. *In vitro* transcription of digoxigenin-labeled probes was performed using the DIG RNA Labeling Kit (Millipore Sigma) according to the manufacturer's instructions. Embryos were dechorionated at the appropriate developmental stages and fixed in 4% paraformaldehyde in phosphate buffered saline (PBS; pH 7.4) for 2 h at room temperature and overnight at 4°C. Whole-mount ISH was performed as previously described (Thisse and Thisse, 2008). After staining, embryos were cleared in 80% glycerol for imaging. Sense probes were used as controls and did not reveal any staining. Images were acquired using an Olympus SZX16 stereomicroscope equipped with an Olympus DP80 dual color camera and Cellsens standard software. Digital images were cropped and aligned using Adobe Illustrator.

Quantification of retinal gene expression

Quantification of gene expression in the retina was carried out according to Picker and Brand (2005) with the following modifications: eyes were dissected from embryos stained by ISH using a sharpened tungsten needle and imaged in 80% glycerol in a lateral view as described above. Images were imported into Fiji ImageJ analysis software (Schindelin et al., 2012; Schneider et al., 2012), transformed to 8-bit grayscale images and inverted. An oval selection was applied half-way between the lens and the RGC layer periphery, and signal intensity was measured along a 360° trajectory using the 'Oval Profile Plot' plugin. Values were exported and analyzed in Microsoft Excel.

Immunolabeling

Larvae were fixed in 4% paraformaldehyde in PBS for 2 h at room temperature and then overnight at 4°C. Larvae were washed three times in PBT (PBS+0.5% Triton X-100). Antigen retrieval was carried out in 150 mM Tris (pH 9) for 5 min at room temperature followed by 20 min at 70°C. Larvae were then permeabilized at room temperature for 15 min in water first, and then for 30 min in PBS with 1% Triton and 0.1% collagenase. Larvae were blocked for 1 h at room temperature with blocking buffer [PBS with 0.5% Triton, 1% DMSO, 1% bovine serum albumin (BSA), and 2% normal goat serum]. Primary anti-EGFP (ab290, Abcam) and anti-TagRFP (M204-3, MBL International) antibodies were applied at 1:500 dilution in PBT supplemented with 1% DMSO and 1% BSA overnight for 4°C. Larvae were washed three times in PBT. Secondary Alexa Fluor 488 goat anti-rabbit (111-545-003, Jackson ImmunoResearch) and Alexa Fluor 594 donkey anti-mouse (715-585-150, Jackson ImmunoResearch) antibodies were diluted 1:500 in PBT with 1% DMSO

Development (2021) 148, dev199584. doi:10.1242/dev.199584

and 1% BSA and applied together with TO-PRO-3 (T3605, Thermo Fisher Scientific) diluted 1:1000 overnight at 4°C. Larvae were washed five times in PBT and mounted in 1% ultrapure low melting point (LMP) agarose (16520050, Thermo Fisher Scientific) for confocal imaging.

Confocal microscopy

For time-course imaging of live larvae from 3 to 6 dpf, larvae were anesthetized in 0.015% tricaine-S and embedded dorsally in 1% LMP agarose in E3 medium+PTU in a lumox membrane-bottomed dish (Greiner Bio-one). Images were acquired on a Leica TCS SP8X laser-scanning confocal microscope equipped with LASX software, HyD detectors and a 20× objective. *z*-series of the entire retinotectal system were acquired at 512×512 pixel resolution with a zoom of 1 and *z*-intervals of 1.5 µm. After imaging, larvae were kept individually in a 12-well dish and allowed to recover for 24 h before being re-anesthetized and mounted dorsally for the next day of imaging. Maximal and sum intensity projections were compiled at each time point in ImageJ software.

For high resolution imaging of the retinotectal system at 4 dpf, immunolabeled larvae were mounted either laterally after removing the contralateral eye or dorsally in 1% LMP agarose and imaged as described above with a *z*-interval of 1 µm. 3D reconstructions of the retinotectal system were generated using FluoRender (Wan et al., 2012, 2017).

Quantification of topographic mapping at the tectum

All quantitative analyses of topographic mapping were conducted using ImageJ software. For unbiased analysis, dorsal view *z*-series were consistently rotated along the *x*, *y* and *z*-axes using the TransformJ Plugin (Meijering et al., 2001), so that the left and right tecta were aligned horizontally, both optic tracts intersected at an angle of 60° and the roundness of the right tectal neuropil was equal to 1. To analyze the area of coverage, rotated images were maximally projected and binarized using a threshold of 80 for TagRFP and of 75 for EGFP. Thresholds were chosen to best represent the raw images acquired. Using the TagRFP channel, we delineated the anterior tectal boundary as the anterior line where retinal axons enter the tectum, and the TagRFP posterior boundary. Using the EGFP channel, we delineated the posterior tectal boundary as the caudal-most border where retinal axons arborize at the tectum. We defined the equator as half the length of the tectum measured along the A/P axis between the anterior and posterior tectal boundaries. We used the 'Analyze Particles' tool in ImageJ to measure the tectal coverage (area) of the TagRFP-positive temporal axons, of the EGFP-positive nasal axons in the anterior half of the tectum (rostral to the equator) and of the EGFP-positive nasal axons in the posterior half of the tectum (caudal to the equator). We calculated the total tectal coverage as the sum of the TagRFP and posterior-EGFP axonal coverages. To further analyze retinotopic mapping along the A/P axis, we established NAMI as the ratio between the EGFP area of coverage in the anterior half of the tectum and the EGFP area of coverage in the posterior half of the tectum. We calculated a refinement index as the ratio change of the NAMI between two consecutive days.

To quantify the sharpness of the boundary between the TagRFP and EGFP projection domains, rotated images were sum-projected for measuring the mean fluorescence intensity of the TagRFP and EGFP signals. We divided the A/P length of the tectum into 10 bins of equal height on merged images using the 'Polygon Selection' tool in ImageJ, and measured the mean fluorescence intensity of each channel in each bin using the 'Measurement' function in ImageJ. Bin 1 was defined as the anterior-most tectal bin and bin10 as the posterior-most tectal bin. Intensity values were normalized to the maximum value for each channel and plotted along the antero-posterior axis. We determined the point at which fluorescence intensity reached 50% of its normalized maximum value for each channel, and defined the sharpness index as the absolute distance between the $EGFP_{50\%}$ and $TagRFP_{50\%}$ positions at 4 and 5 dpf (see Fig. S3 for a detailed illustration of our quantifications).

Statistical analysis

All statistical analyses were performed using GraphPad Prism 9 software. We define biological replicates as individual larvae from a mixed clutch born from pairings of at least two males and two females. Each experiment was repeated under similar experimental conditions. Sample size was decided based on the low variability detected in pilot studies. Data are presented as mean±s.e.m. For better communicating variability across samples and experimental reproducibility, graphs are represented as 'SuperPlots' (Lord et al., 2020), in which biological replicates representing independent experiments are color-coded, with circles representing individual larvae tested and triangles representing averages. We compared groups with repeated measures over time (Fig. 5F-K) using repeated measures one-way ANOVA with Tukey's multiple comparisons post-hoc test. We analyzed the refinement index using a two-tailed, paired *t*-test compared with 1 (1 representing no change). We analyzed the sharpness index in Fig. 5P using a two-tailed, paired *t*-test, and the EGFP mean distribution in Fig. 5M using a two-tailed, paired *t*-test within each bin. We compared data with both 'within-subjects' and 'between-subjects' factors (Fig. 6G-M) using mixed effects one-way ANOVA followed by Tukey's multiple comparisons post-hoc test. The number of larvae analyzed are described for each experiment in the figure legends. In all figures, $*P<0.05$, $**P<0.01$ and $***P<0.001$.

Acknowledgements

We thank the expert help of Dr Edsel Pena (University of South Carolina) for assistance with statistical analyses, and Quill Thomas for technical assistance and fish husbandry.

Competing interests

The authors declare no competing or financial interests.

Author contributions

Conceptualization: F.E.P.; Methodology: O.S.; Validation: O.S., C.J.W., T.M., F.E.P.; Formal analysis: O.S., C.J.W., T.M., F.E.P.; Investigation: O.S., F.E.P.; Resources: F.E.P.; Data curation: O.S., C.J.W., T.M., F.E.P.; Writing - original draft: O.S.; Writing - review & editing: C.J.W., F.E.P.; Visualization: O.S., C.J.W., T.M., F.E.P.; Supervision: F.E.P.; Project administration: F.E.P.; Funding acquisition: F.E.P.

Funding

This work was supported by the National Institutes of Health/National Institute of Neurological Disorders and Stroke (R01NS109197 to F.E.P.), the University of South Carolina SmartState Center in Childhood Neurotherapeutics (to F.E.P.) and an Aspire I grant from the Office of the Vice President for Research at the University of South Carolina (to F.E.P.). Deposited in PMC for release after 12 months.

Peer review history

The peer review history is available online at https://journals.biologists.com/dev/article-lookup/doi/10.1242/dev.199584.

References

Adamska, M., Wolff, A., Kreusler, M., Wittbrodt, J., Braun, T. and Bober, E. (2001). Five Nkx5 genes show differential expression patterns in anlagen of sensory organs in medaka: insight into the evolution of the gene family. *Dev. Genes Evol.* **211**, 338-349. doi:10.1007/s004270100162

Alsina, B., Vu, T. and Cohen-Cory, S. (2001). Visualizing synapse formation in arborizing optic axons in vivo: dynamics and modulation by BDNF. *Nat. Neurosci.* **4**, 1093-1101. doi:10.1038/nn735

Baeriswyl, T. and Stoeckli, E. T. (2008). Axonin-1/TAG-1 is required for pathfinding of granule cell axons in the developing cerebellum. *Neural Dev.* **3**, 7. doi:10.1186/1749-8104-3-7

Baier, H., Klostermann, S., Trowe, T., Karlstrom, R. O., Nüsslein-Volhard, C. and Bonhoeffer, F. (1996). Genetic dissection of the retinotectal projection. *Development* **123**, 415-425. doi:10.1242/dev.123.1.415

Ben Fredj, N., Hammond, S., Otsuna, H., Chien, C. B., Burrone, J. and Meyer, M. P. (2010). Synaptic activity and activity-dependent competition regulates axon arbor maturation, growth arrest, and territory in the retinotectal projection. *J. Neurosci.* **30**, 10939-10951. doi:10.1523/JNEUROSCI.1556-10.2010

Benjumeda, I., Escalante, A., Law, C., Morales, D., Chauvin, G., Muça, G., Coca, Y., Márquez, J., López-Bendito, G., Kania, A. et al. (2013). Uncoupling of EphA/ephrinA signaling and spontaneous activity in neural circuit wiring. *J. Neurosci.* **33**, 18208-18218. doi:10.1523/JNEUROSCI.1931-13.2013

Biehlmaier, O., Neuhauss, S. C. and Kohler, K. (2001). Onset and time course of apoptosis in the developing zebrafish retina. *Cell Tissue Res.* **306**, 199-207. doi:10.1007/s004410100447

Bogdanovic, O., Fernandez-Minan, A., Tena, J. J., de la Calle-Mustienes, E., Hidalgo, C., van Kruysbergen, I., van Heeringen, S. J., Veenstra, G. J. and

Gomez-Skarmeta, J. L. (2012). Dynamics of enhancer chromatin signatures mark the transition from pluripotency to cell specification during embryogenesis. *Genome Res.* **22**, 2043-2053. doi:10.1101/gr.134833.111

Boisset, G. and Schorderet, D. F. (2012). Zebrafish hmx1 promotes retinogenesis. *Exp. Eye Res.* **105**, 34-42. doi:10.1016/j.exer.2012.10.002

Bonn, S., Zinzen, R. P., Girardot, C., Gustafson, E. H., Perez-Gonzalez, A., Delhomme, N., Ghavi-Helm, Y., Wilczyński, B., Riddell, A. and Furlong, E. E. (2012). Tissue-specific analysis of chromatin state identifies temporal signatures of enhancer activity during embryonic development. *Nat. Genet.* **44**, 148-156. doi:10.1038/ng.1064

Buchstaller, A., Kunz, S., Berger, P., Kunz, B., Ziegler, U., Rader, C. and Sonderegger, P. (1996). Cell adhesion molecules NgCAM and axonin-1 form heterodimers in the neuronal membrane and cooperate in neurite outgrowth promotion. *J. Cell Biol.* **135**, 1593-1607. doi:10.1083/jcb.135.6.1593

Burbridge, T. J., Xu, H. P., Ackman, J. B., Ge, X., Zhang, Y., Ye, M. J., Zhou, Z. J., Xu, J., Contractor, A. and Crair, M. C. (2014). Visual circuit development requires patterned activity mediated by retinal acetylcholine receptors. *Neuron* **84**, 1049-1064. doi:10.1016/j.neuron.2014.10.051

Burrill, J. D. and Easter, S. S.Jr. (1995). The first retinal axons and their microenvironment in zebrafish: cryptic pioneers and the pretract. *J. Neurosci.* **15**, 2935-2947. doi:10.1523/JNEUROSCI.15-04-02935.1995

Campbell, D. S., Stringham, S. A., Timm, A., Xiao, T., Law, M. Y., Baier, H., Nonet, M. L. and Chien, C. B. (2007). Slit1a inhibits retinal ganglion cell arborization and synaptogenesis via Robo2-dependent and -independent pathways. *Neuron* **55**, 231-245. doi:10.1016/j.neuron.2007.06.034

Cang, J. and Feldheim, D. A. (2013). Developmental mechanisms of topographic map formation and alignment. *Annu. Rev. Neurosci.* **36**, 51-77. doi:10.1146/annurev-neuro-062012-170341

Cang, J., Rentería, R. C., Kaneko, M., Liu, X., Copenhagen, D. R. and Stryker, M. P. (2005). Development of precise maps in visual cortex requires patterned spontaneous activity in the retina. *Neuron* **48**, 797-809. doi:10.1016/j.neuron.2005.09.015

Cang, J., Wang, L., Stryker, M. P. and Feldheim, D. A. (2008). Roles of ephrin-as and structured activity in the development of functional maps in the superior colliculus. *J. Neurosci.* **28**, 11015-11023. doi:10.1523/JNEUROSCI.2478-08.2008

Carmean, V., Yonkers, M. A., Tellez, M. B., Willer, J. R., Willer, G. B., Gregg, R. G., Geisler, R., Neuhauss, S. C. and Ribera, A. B. (2015). pigk Mutation underlies macho behavior and affects Rohon-Beard cell excitability. *J. Neurophysiol.* **114**, 1146-1157. doi:10.1152/jn.00355.2015

Chandrasekaran, A. R., Plas, D. T., Gonzalez, E. and Crair, M. C. (2005). Evidence for an instructive role of retinal activity in retinotopic map refinement in the superior colliculus of the mouse. *J. Neurosci.* **25**, 6929-6938. doi:10.1523/JNEUROSCI.1470-05.2005

Chen, C., Westenbroek, R. E., Xu, X., Edwards, C. A., Sorenson, D. R., Chen, Y., McEwen, D. P., O'Malley, H. A., Bharucha, V., Meadows, L. S. et al. (2004). Mice lacking sodium channel beta1 subunits display defects in neuronal excitability, sodium channel expression, and nodal architecture. *J. Neurosci.* **24**, 4030-4042. doi:10.1523/JNEUROSCI.4139-03.2004

Cohen-Cory, S. (1999). BDNF modulates, but does not mediate, activity-dependent branching and remodeling of optic axon arbors in vivo. *J. Neurosci.* **19**, 9996-10003. doi:10.1523/JNEUROSCI.19-22-09996.1999

Cole, L. K. and Ross, L. S. (2001). Apoptosis in the developing zebrafish embryo. *Dev. Biol.* **240**, 123-142. doi:10.1006/dbio.2001.0432

Cowan, C. S., Renner, M., De Gennaro, M., Gross-Scherf, B., Goldblum, D., Hou, Y., Munz, M., Rodrigues, T. M., Krol, J., Szikra, T. et al. (2020). Cell types of the human retina and its organoids at single-cell resolution. *Cell* **182**, 1623-1640.e1634. doi:10.1016/j.cell.2020.08.013

Dahlem, T. J., Hoshijima, K., Jurynec, M. J., Gunther, D., Starker, C. G., Locke, A. S., Weis, A. M., Voytas, D. F. and Grunwald, D. J. (2012). Simple methods for generating and detecting locus-specific mutations induced with TALENs in the zebrafish genome. *PLoS Genet.* **8**, e1002861. doi:10.1371/journal.pgen.1002861

Dang, P., Smythe, E. and Furley, A. J. W. (2012). TAG1 regulates the endocytic trafficking and signaling of the semaphorin3A receptor complex. *J. Neurosci.* **32**, 10370-10382. doi:10.1523/JNEUROSCI.5874-11.2012

Deitcher, D. L., Fekete, D. M. and Cepko, C. L. (1994). Asymmetric expression of a novel homeobox gene in vertebrate sensory organs. *J. Neurosci.* **14**, 486-498. doi:10.1523/JNEUROSCI.14-02-00486.1994

Dhande, O. S., Hua, E. W., Guh, E., Yeh, J., Bhatt, S., Zhang, Y., Ruthazer, E. S., Feller, M. B. and Crair, M. C. (2011). Development of single retinofugal axon arbors in normal and β2 knock-out mice. *J. Neurosci.* **31**, 3384-3399. doi:10.1523/JNEUROSCI.4899-10.2011

Fitzli, D., Stoeckli, E. T., Kunz, S., Siribour, K., Rader, C., Kunz, B., Kozlov, S. V., Buchstaller, A., Lane, R. P., Suter, D. M. et al. (2000). A direct interaction of axonin-1 with NgCAM-related cell adhesion molecule (NrCAM) results in guidance, but not growth of commissural axons. *J. Cell Biol.* **149**, 951-968. doi:10.1083/jcb.149.4.951

Förster, D., Helmbrecht, T. O., Mearns, D. S., Jordan, L., Mokayes, N. and Baier, H. (2020). Retinotectal circuitry of larval zebrafish is adapted to detection and pursuit of prey. *Elife* **9**, e58596. doi:10.7554/eLife.58596.sa2

Gillespie, R. L., Urquhart, J., Lovell, S. C., Biswas, S., Parry, N. R., Schorderet, D. F., Lloyd, I. C., Clayton-Smith, J. and Black, G. C. (2015). Abrogation of HMX1 function causes rare oculoauricular syndrome associated with congenital cataract, anterior segment dysgenesis, and retinal dystrophy. *Invest. Ophthalmol. Vis. Sci.* **56**, 883-891. doi:10.1167/iovs.14-15861

Gnuegge, L., Schmid, S. and Neuhauss, S. C. (2001). Analysis of the activity-deprived zebrafish mutant macho reveals an essential requirement of neuronal activity for the development of a fine-grained visuotopic map. *J. Neurosci.* **21**, 3542-3548. doi:10.1523/JNEUROSCI.21-10-03542.2001

Gosse, N. J., Nevin, L. M. and Baier, H. (2008). Retinotopic order in the absence of axon competition. *Nature* **452**, 892-895. doi:10.1038/nature06816

Granato, M., van Eeden, F. J., Schach, U., Trowe, T., Brand, M., Furutani-Seiki, M., Haffter, P., Hammerschmidt, M., Heisenberg, C. P., Jiang, Y. J. et al. (1996). Genes controlling and mediating locomotion behavior of the zebrafish embryo and larva. *Development* **123**, 399-413. doi:10.1242/dev.123.1.399

Gurung, S., Asante, E., Hummel, D., Williams, A., Feldman-Schultz, O., Halloran, M. C., Sittaramane, V. and Chandrasekhar, A. (2018). Distinct roles for the cell adhesion molecule Contactin2 in the development and function of neural circuits in zebrafish. *Mech. Dev.* **152**, 1-12. doi:10.1016/j.mod.2018.05.005

Harvey, B. M., Baxter, M. and Granato, M. (2019). Optic nerve regeneration in larval zebrafish exhibits spontaneous capacity for retinotopic but not tectum specific axon targeting. *PLoS ONE* **14**, e0218667. doi:10.1371/journal.pone.0218667

Heintzman, N. D., Stuart, R. K., Hon, G., Fu, Y., Ching, C. W., Hawkins, R. D., Barrera, L. O., Van Calcar, S., Qu, C., Ching, K. A. et al. (2007). Distinct and predictive chromatin signatures of transcriptional promoters and enhancers in the human genome. *Nat. Genet.* **39**, 311-318. doi:10.1038/ng1966

Hiramoto, M. and Cline, H. T. (2014). Optic flow instructs retinotopic map formation through a spatial to temporal to spatial transformation of visual information. *Proc. Natl. Acad. Sci. USA* **111**, E5105-E5113. doi:10.1073/pnas.1416953111

Hoshijima, K., Jurynec, M. J., Klatt Shaw, D., Jacobi, A. M., Behlke, M. A. and Grunwald, D. J. (2019). Highly efficient CRISPR-Cas9-based methods for generating deletion mutations and F0 embryos that lack gene function in Zebrafish. *Dev. Cell* **51**, 645-657.e644. doi:10.1016/j.devcel.2019.10.004

Hu, M. and Easter, S. S. (1999). Retinal neurogenesis: the formation of the initial central patch of postmitotic cells. *Dev. Biol.* **207**, 309-321. doi:10.1006/dbio.1998.9031

Hua, J. Y., Smear, M. C., Baier, H. and Smith, S. J. (2005). Regulation of axon growth in vivo by activity-based competition. *Nature* **434**, 1022-1026. doi:10.1038/nature03409

Irimia, M., Tena, J. J., Alexis, M. S., Fernandez-Miñan, A., Maeso, I., Bogdanovic, O., de la Calle-Mustienes, E., Roy, S. W., Gómez-Skarmeta, J. L. and Fraser, H. B. (2012). Extensive conservation of ancient microsynteny across metazoans due to cis-regulatory constraints. *Genome Res.* **22**, 2356-2367. doi:10.1101/gr.139725.112

Jacobi, A. M., Rettig, G. R., Turk, R., Collingwood, M. A., Zeiner, S. A., Quadros, R. M., Harms, D. W., Bonthuis, P. J., Gregg, C., Ohtsuka, M. et al. (2017). Simplified CRISPR tools for efficient genome editing and streamlined protocols for their delivery into mammalian cells and mouse zygotes. *Methods* **121-122**, 16-28. doi:10.1016/j.ymeth.2017.03.021

Kaethner, R. J. and Stuermer, C. A. (1992). Dynamics of terminal arbor formation and target approach of retinotectal axons in living zebrafish embryos: a time-lapse study of single axons. *J. Neurosci.* **12**, 3257-3271. doi:10.1523/JNEUROSCI.12-08-03257.1992

Kaethner, R. J. and Stuermer, C. A. (1994). Growth behavior of retinotectal axons in live zebrafish embryos under TTX-induced neural impulse blockade. *J. Neurobiol.* **25**, 781-796. doi:10.1002/neu.480250704

Kawakami, K. (2007). Tol2: a versatile gene transfer vector in vertebrates. *Genome Biol.* **8** Suppl. 1, S7. doi:10.1186/gb-2007-8-s1-s7

Kawakami, K., Shima, A. and Kawakami, N. (2000). Identification of a functional transposase of the Tol2 element, an Ac-like element from the Japanese medaka fish, and its transposition in the zebrafish germ lineage. *Proc. Natl. Acad. Sci. USA.* **97**, 11403-11408. doi:10.1073/pnas.97.21.11403

Kawakami, K., Asakawa, K., Hibi, M., Itoh, M., Muto, A. and Wada, H. (2016). Gal4 Driver transgenic zebrafish: powerful tools to study developmental biology, organogenesis, and neuroscience. *Adv. Genet.* **95**, 65-87. doi:10.1016/bs.adgen.2016.04.002

Kazarinova-Noyes, K., Malhotra, J. D., McEwen, D. P., Mattei, L. N., Berglund, E. O., Ranscht, B., Levinson, S. R., Schachner, M., Shrager, P., Isom, L. L. et al. (2001). Contactin associates with Na+ channels and increases their functional expression. *J. Neurosci.* **21**, 7517-7525. doi:10.1523/JNEUROSCI.21-19-07517.2001

Kent, W. J., Sugnet, C. W., Furey, T. S., Roskin, K. M., Pringle, T. H., Zahler, A. M. and Haussler, D. (2002). The human genome browser at UCSC. *Genome Res.* **12**, 996-1006. doi:10.1101/gr.229102

Kimmel, C. B., Ballard, W. W., Kimmel, S. R., Ullmann, B. and Schilling, T. F. (1995). Stages of embryonic development of the zebrafish. *Dev. Dyn.* **203**, 253-310. doi:10.1002/aja.1002030302

Kita, E. M., Scott, E. K. and Goodhill, G. J. (2015). Topographic wiring of the retinotectal connection in zebrafish. *Dev. Neurobiol.* **75**, 542-556. doi:10.1002/dneu.22256

Kobayashi, T., Nakamura, H. and Yasuda, M. (1990). Disturbance of refinement of retinotectal projection in chick embryos by tetrodotoxin and grayanotoxin. *Brain Res. Dev. Brain Res.* **57**, 29-35. doi:10.1016/0165-3806(90)90181-W

Kuhn, T. B., Stoeckli, E. T., Condrau, M. A., Rathjen, F. G. and Sonderegger, P. (1991). Neurite outgrowth on immobilized axonin-1 is mediated by a heterophilic interaction with L1(G4). *J. Cell Biol.* **115**, 1113-1126. doi:10.1083/jcb.115.4.1113

Kunz, S., Spirig, M., Ginsburg, C., Buchstaller, A., Berger, P., Lanz, R., Rader, C., Vogt, L., Kunz, B. and Sonderegger, P. (1998). Neurite fasciculation mediated by complexes of axonin-1 and Ng cell adhesion molecule. *J. Cell Biol.* **143**, 1673-1690. doi:10.1083/jcb.143.6.1673

Kutsarova, E., Munz, M. and Ruthazer, E. S. (2016). Rules for shaping neural connections in the developing brain. *Front. Neural Circuits* **10**, 111. doi:10.3389/fncir.2016.00111

Kwan, K. M., Fujimoto, E., Grabher, C., Mangum, B. D., Hardy, M. E., Campbell, D. S., Parant, J. M., Yost, H. J., Kanki, J. P. and Chien, C. B. (2007). The Tol2kit: a multisite gateway-based construction kit for Tol2 transposon transgenesis constructs. *Dev. Dyn.* **236**, 3088-3099. doi:10.1002/dvdy.21343

Kwan, K. M., Otsuna, H., Kidokoro, H., Carney, K. R., Saijoh, Y. and Chien, C. B. (2012). A complex choreography of cell movements shapes the vertebrate eye. *Development* **139**, 359-372. doi:10.1242/dev.071407

Laessing, U. and Stuermer, C. A. (1996). Spatiotemporal pattern of retinal ganglion cell differentiation revealed by the expression of neurolin in embryonic zebrafish. *J. Neurobiol.* **29**, 65-74. doi:10.1002/(SICI)1097-4695(199601)29:1<65::AID-NEU5>3.0.CO;2-5

Lang, D. M., Warren, J. T., Jr, Klisa, C. and Stuermer, C. A. (2001). Topographic restriction of TAG-1 expression in the developing retinotectal pathway and target dependent reexpression during axon regeneration. *Mol. Cell. Neurosci.* **17**, 398-414. doi:10.1006/mcne.2000.0936

Law, C. O., Kirby, R. J., Aghamohammadzadeh, S. and Furley, A. J. (2008). The neural adhesion molecule TAG-1 modulates responses of sensory axons to diffusible guidance signals. *Development* **135**, 2361-2371. doi:10.1242/dev.009019

Leighton, A. H. and Lohmann, C. (2016). The wiring of developing sensory circuits-from patterned spontaneous activity to synaptic plasticity mechanisms. *Front. Neural Circuits* **10**, 71. doi:10.3389/fncir.2016.00071

Liu, C. J., Dib-Hajj, S. D., Black, J. A., Greenwood, J., Lian, Z. and Waxman, S. G. (2001). Direct interaction with contactin targets voltage-gated sodium channel Na(v)1.9/NaN to the cell membrane. *J. Biol. Chem.* **276**, 46553-46561. doi:10.1074/jbc.M108699200

Lord, S. J., Velle, K. B., Mullins, R. D. and Fritz-Laylin, L. K. (2020). SuperPlots: communicating reproducibility and variability in cell biology. *J. Cell Biol.* **219**, e202001064. doi:10.1083/jcb.202001064

Louail, A., Sierksma, M. C., Chaffiol, A., Baudet, S., Assali, A., Couvet, S., Nedjam, M., Roche, F., Zagar, Y., Duebel, J. et al. (2020). cAMP-Dependent co-stabilization of axonal arbors from adjacent developing neurons. *Cell Rep.* 33, 108220. doi:10.1016/j.celrep.2020.108220

Lukowski, S. W., Lo, C. Y., Sharov, A. A., Nguyen, Q., Fang, L., Hung, S. S. C., Zhu, L., Zhang, T., Grünert, U., Nguyen, T. et al. (2019). A single-cell transcriptome atlas of the adult human retina. *EMBO J.* **38**, e100811. doi:10.15252/embj.2018100811

Ma, Q.-H., Futagawa, T., Yang, W.-L., Jiang, X.-D., Zeng, L., Takeda, Y., Xu, R.-X., Bagnard, D., Schachner, M., Furley, A. J. et al. (2008). A TAG1-APP signalling pathway through Fe65 negatively modulates neurogenesis. *Nat. Cell Biol.* **10**, 283-294. doi:10.1038/ncb1690

Masuda, T. (2017). Contactin-2/TAG-1, active on the front line for three decades. *Cell Adh. Migr.* **11**, 524-531. doi:10.1080/19336918.2016.1269998

McEwen, D. P. and Isom, L. L. (2004). Heterophilic interactions of sodium channel beta1 subunits with axonal and glial cell adhesion molecules. *J. Biol. Chem.* **279**, 52744-52752. doi:10.1074/jbc.M405990200

McEwen, D. P., Meadows, L. S., Chen, C., Thyagarajan, V. and Isom, L. L. (2004). Sodium channel β1 subunit-mediated modulation of Nav1.2 currents and cell surface density is dependent on interactions with contactin and ankyrin. *J. Biol. Chem.* **279**, 16044-16049. doi:10.1074/jbc.M400856200

Meijering, E. H., Niessen, W. J. and Viergever, M. A. (2001). Quantitative evaluation of convolution-based methods for medical image interpolation. *Med. Image Anal.* **5**, 111-126. doi:10.1016/S1361-8415(00)00040-2

Meyer, M. P. and Smith, S. J. (2006). Evidence from in vivo imaging that synaptogenesis guides the growth and branching of axonal arbors by two distinct mechanisms. *J. Neurosci.* **26**, 3604-3614. doi:10.1523/JNEUROSCI.0223-06.2006

Mohebiany, A. N., Harroch, S. and Bouyain, S. (2014). New insights into the roles of the contactin cell adhesion molecules in neural development. *Adv. Neurobiol.* **8**, 165-194. doi:10.1007/978-1-4614-8090-7_8

Moriyoshi, K., Richards, L. J., Akazawa, C., O'Leary, D. D. and Nakanishi, S. (1996). Labeling neural cells using adenoviral gene transfer of membrane-targeted GFP. *Neuron* **16**, 255-260. doi:10.1016/S0896-6273(00)80044-6

Mosimann, C., Kaufman, C. K., Li, P., Pugach, E. K., Tamplin, O. J. and Zon, L. I. (2011). Ubiquitous transgene expression and Cre-based recombination driven by the ubiquitin promoter in zebrafish. *Development* **138**, 169-177. doi:10.1242/dev.059345

Munroe, R. J., Prabhu, V., Acland, G. M., Johnson, K. R., Harris, B. S., O'Brien, T. P., Welsh, I. C., Noden, D. M. and Schimenti, J. C. (2009). Mouse H6 Homeobox 1 (Hmx1) mutations cause cranial abnormalities and reduced body mass. *BMC Dev. Biol.* **9**, 27. doi:10.1186/1471-213X-9-27

Munz, M., Gobert, D., Schohl, A., Poquérusse, J., Podgorski, K., Spratt, P. and Ruthazer, E. S. (2014). Rapid Hebbian axonal remodeling mediated by visual stimulation. *Science* **344**, 904-909. doi:10.1126/science.1251593

Ohishi, K., Inoue, N., Maeda, Y., Takeda, J., Riezman, H. and Kinoshita, T. (2000). Gaa1p and gpi8p are components of a glycosylphosphatidylinositol (GPI) transamidase that mediates attachment of GPI to proteins. *Mol. Biol. Cell* **11**, 1523-1533. doi:10.1091/mbc.11.5.1523

O'Rourke, N. A. and Fraser, S. E. (1990). Dynamic changes in optic fiber terminal arbors lead to retinotopic map formation: an in vivo confocal microscopic study. *Neuron* **5**, 159-171. doi:10.1016/0896-6273(90)90306-Z

Parant, J. M., George, S. A., Pryor, R., Wittwer, C. T. and Yost, H. J. (2009). A rapid and efficient method of genotyping zebrafish mutants. *Dev. Dyn.* **238**, 3168-3174. doi:10.1002/dvdy.22143

Pfeiffenberger, C., Yamada, J. and Feldheim, D. A. (2006). Ephrin-As and patterned retinal activity act together in the development of topographic maps in the primary visual system. *J. Neurosci.* **26**, 12873-12884. doi:10.1523/JNEUROSCI.3595-06.2006

Picker, A. and Brand, M. (2005). Fgf signals from a novel signaling center determine axial patterning of the prospective neural retina. *Development* **132**, 4951-4962. doi:10.1242/dev.02071

Pierre, K., Dupouy, B., Allard, M., Poulain, D. A. and Theodosis, D. T. (2001). Mobilization of the cell adhesion glycoprotein F3/contactin to axonal surfaces is activity dependent. *Eur. J. Neurosci.* **14**, 645-656. doi:10.1046/j.0953-816x.2001.01682.x

Pittman, A. J., Law, M. Y. and Chien, C. B. (2008). Pathfinding in a large vertebrate axon tract: isotypic interactions guide retinotectal axons at multiple choice points. *Development* **135**, 2865-2871. doi:10.1242/dev.025049

Portugues, R., Severi, K. E., Wyart, C. and Ahrens, M. B. (2013). Optogenetics in a transparent animal: circuit function in the larval zebrafish. *Curr. Opin. Neurobiol.* **23**, 119-126. doi:10.1016/j.conb.2012.11.001

Poulain, F. E. and Chien, C. B. (2013). Proteoglycan-mediated axon degeneration corrects pretarget topographic sorting errors. *Neuron* **78**, 49-56. doi:10.1016/j.neuron.2013.02.005

Poulain, F. E., Gaynes, J. A., Stacher Hörndli, C., Law, M. Y. and Chien, C. B. (2010). Analyzing retinal axon guidance in zebrafish. *Methods Cell Biol.* **100**, 3-26. doi:10.1016/B978-0-12-384892-5.00001-3

Rada-Iglesias, A., Bajpai, R., Swigut, T., Brugmann, S. A., Flynn, R. A. and Wysocka, J. (2011). A unique chromatin signature uncovers early developmental enhancers in humans. *Nature* **470**, 279-283. doi:10.1038/nature09692

Rahman, T. N., Munz, M., Kutsarova, E., Bilash, O. M. and Ruthazer, E. S. (2020). Stentian structural plasticity in the developing visual system. *Proc. Natl. Acad. Sci. USA* **117**, 10636-10638. doi:10.1073/pnas.2001107117

Reh, T. A. and Constantine-Paton, M. (1985). Eye-specific segregation requires neural activity in three-eyed Rana pipiens. *J. Neurosci.* **5**, 1132-1143. doi:10.1523/JNEUROSCI.05-05-01132.1985

Ribera, A. B. and Nüsslein-Volhard, C. (1998). Zebrafish touch-insensitive mutants reveal an essential role for the developmental regulation of sodium current. *J. Neurosci.* **18**, 9181-9191. doi:10.1523/JNEUROSCI.18-22-09181.1998

Robles, E. (2017). The power of projectomes: genetic mosaic labeling in the larval zebrafish brain reveals organizing principles of sensory circuits. *J. Neurogenet.* **31**, 61-69. doi:10.1080/01677063.2017.1359834

Rush, A. M., Craner, M. J., Kageyama, T., Dib-Hajj, S. D., Waxman, S. G. and Ranscht, B. (2005). Contactin regulates the current density and axonal expression of tetrodotoxin-resistant but not tetrodotoxin-sensitive sodium channels in DRG neurons. *Eur. J. Neurosci.* **22**, 39-49. doi:10.1111/j.1460-9568.2005.04186.x

Ruthazer, E. S., Akerman, C. J. and Cline, H. T. (2003). Control of axon branch dynamics by correlated activity in vivo. *Science* **301**, 66-70. doi:10.1126/science.1082545

Ruthazer, E. S., Li, J. and Cline, H. T. (2006). Stabilization of axon branch dynamics by synaptic maturation. *J. Neurosci.* **26**, 3594-3603. doi:10.1523/JNEUROSCI.0069-06.2006

Schindelin, J., Arganda-Carreras, I., Frise, E., Kaynig, V., Longair, M., Pietzsch, T., Preibisch, S., Rueden, C., Saalfeld, S., Schmid, B. et al. (2012). Fiji: an open-source platform for biological-image analysis. *Nat. Methods* **9**, 676-682. doi:10.1038/nmeth.2019

Schmitt, E. A. and Dowling, J. E. (1999). Early retinal development in the zebrafish, Danio rerio: light and electron microscopic analyses. *J. Comp. Neurol.* **404**,

515-536. doi:10.1002/(SICI)1096-9861(19990222)404:4<515::AID-CNE8>3.0.CO;2-A

Schmidt, J. T., Buzzard, M., Borress, R. and Dhillon, S. (2000). MK801 increases retinotectal arbor size in developing zebrafish without affecting kinetics of branch elimination and addition. *J. Neurobiol.* **42**, 303-314. doi:10.1002/(SICI)1097-4695(20000215)42:3<303::AID-NEU2>3.0.CO;2-A

Schneider, C. A., Rasband, W. S. and Eliceiri, K. W. (2012). NIH Image to ImageJ: 25 years of image analysis. *Nat. Methods* **9**, 671-675. doi:10.1038/nmeth.2089

Schorderet, D. F., Nichini, O., Boisset, G., Polok, B., Tiab, L., Mayeur, H., Raji, B., de la Houssaye, G., Abitbol, M. M. and Munier, F. L. (2008). Mutation in the human homeobox gene NKX5-3 causes an oculo-auricular syndrome. *Am. J. Hum. Genet.* **82**, 1178-1184. doi:10.1016/j.ajhg.2008.03.007

Schulte, D. and Cepko, C. L. (2000). Two homeobox genes define the domain of EphA3 expression in the developing chick retina. *Development* **127**, 5033-5045. doi:10.1242/dev.127.23.5033

Shah, B. S., Rush, A. M., Liu, S., Tyrrell, L., Black, J. A., Dib-Hajj, S. D. and Waxman, S. G. (2004). Contactin associates with sodium channel Nav1.3 in native tissues and increases channel density at the cell surface. *J. Neurosci.* **24**, 7387-7399. doi:10.1523/JNEUROSCI.0322-04.2004

Simpson, H. D., Kita, E. M., Scott, E. K. and Goodhill, G. J. (2013). A quantitative analysis of branching, growth cone turning, and directed growth in zebrafish retinotectal axon guidance. *J. Comp. Neurol.* **521**, 1409-1429. doi:10.1002/cne.23248

Smear, M. C., Tao, H. W., Staub, W., Orger, M. B., Gosse, N. J., Liu, Y., Takahashi, K., Poo, M. M. and Baier, H. (2007). Vesicular glutamate transport at a central synapse limits the acuity of visual perception in zebrafish. *Neuron* **53**, 65-77. doi:10.1016/j.neuron.2006.12.013

Spead, O. and Poulain, F. E. (2020a). Trans-axonal signaling in neural circuit wiring. *Int. J. Mol. Sci.* **21**, 5170. doi:10.3390/ijms21145170

Spead, O. and Poulain, F. E. (2020b). Activity-mediated refinement of nasal retinal projections drives topographic map sharpening in the teleost visual system. *bioRxiv* 422653. doi:10.1101/2020.12.14.422653

Sperry, R. W. (1963). Chemoaffinity in the orderly growth of nerve fiber patterns and connections. *Proc. Natl. Acad. Sci. USA* **50**, 703-710. doi:10.1073/pnas.50.4.703

Stadler, H. S. and Solursh, M. (1994). Characterization of the homeobox-containing gene GH6 identifies novel regions of homeobox gene expression in the developing chick embryo. *Dev. Biol.* **161**, 251-262. doi:10.1006/dbio.1994.1025

Stellwagen, D. and Shatz, C. J. (2002). An instructive role for retinal waves in the development of retinogeniculate connectivity. *Neuron* **33**, 357-367. doi:10.1016/S0896-6273(02)00577-9

Stoeckli, E. T. and Landmesser, L. T. (1995). Axonin-1, Nr-CAM, and Ng-CAM play different roles in the in vivo guidance of chick commissural neurons. *Neuron* **14**, 1165-1179. doi:10.1016/0896-6273(95)90264-3

Stuermer, C. A. (1988). Retinotopic organization of the developing retinotectal projection in the zebrafish embryo. *J. Neurosci.* **8**, 4513-4530. doi:10.1523/JNEUROSCI.08-12-04513.1988

Stuermer, C. A., Rohrer, B. and Münz, H. (1990). Development of the retinotectal projection in zebrafish embryos under TTX-induced neural-impulse blockade. *J. Neurosci.* **10**, 3615-3626. doi:10.1523/JNEUROSCI.10-11-03615.1990

Suetterlin, P. and Drescher, U. (2014). Target-independent ephrina/EphA-mediated axon-axon repulsion as a novel element in retinocollicular mapping. *Neuron* **84**, 740-752. doi:10.1016/j.neuron.2014.09.023

Suter, D. M., Pollerberg, G. E., Buchstaller, A., Giger, R. J., Dreyer, W. J. and Sonderegger, P. (1995). Binding between the neural cell adhesion molecules axonin-1 and Nr-CAM/Bravo is involved in neuron-glia interaction. *J. Cell Biol.* **131**, 1067-1081. doi:10.1083/jcb.131.4.1067

Suter, T., Blagburn, S. V., Fisher, S. E., Anderson-Keightly, H. M., D'Elia, K. P. and Jaworski, A. (2020). TAG-1 Multifunctionality coordinates neuronal migration, axon guidance, and fasciculation. *Cell Rep.* **30**, 1164-1177.e1167. doi:10.1016/j.celrep.2019.12.085

Takahashi, H., Shintani, T., Sakuta, H. and Noda, M. (2003). CBF1 controls the retinotectal topographical map along the anteroposterior axis through multiple mechanisms. *Development* **130**, 5203-5215. doi:10.1242/dev.00724

Takahashi, H., Sakuta, H., Shintani, T. and Noda, M. (2009). Functional mode of FoxD1/CBF2 for the establishment of temporal retinal specificity in the developing chick retina. *Dev. Biol.* **331**, 300-310. doi:10.1016/j.ydbio.2009.05.549

Thisse, C. and Thisse, B. (2008). High-resolution in situ hybridization to whole-mount zebrafish embryos. *Nat. Protoc.* **3**, 59-69. doi:10.1038/nprot.2007.514

Thompson, A., Gribizis, A., Chen, C. and Crair, M. C. (2017). Activity-dependent development of visual receptive fields. *Curr. Opin. Neurobiol.* **42**, 136-143. doi:10.1016/j.conb.2016.12.007

Triplett, J. W. (2014). Molecular guidance of retinotopic map development in the midbrain. *Curr. Opin. Neurobiol.* **24**, 7-12. doi:10.1016/j.conb.2013.07.006

Trowe, T., Klostermann, S., Baier, H., Granato, M., Crawford, A. D., Grunewald, B., Hoffmann, H., Karlstrom, R. O., Meyer, S. U., Müller, B. et al. (1996). Mutations disrupting the ordering and topographic mapping of axons in the retinotectal projection of the zebrafish, Danio rerio. *Development* **123**, 439-450. doi:10.1242/dev.123.1.439

Vaclavik, V., Schorderet, D. F., Borruat, F. X. and Munier, F. L. (2011). Retinal dystrophy in the oculo-auricular syndrome due to HMX1 mutation. *Ophthalmic Genet.* **32**, 114-117. doi:10.3109/13816810.2011.562955

Voigt, A. P., Whitmore, S. S., Flamme-Wiese, M. J., Riker, M. J., Wiley, L. A., Tucker, B. A., Stone, E. M., Mullins, R. F. and Scheetz, T. E. (2019). Molecular characterization of foveal versus peripheral human retina by single-cell RNA sequencing. *Exp. Eye Res.* **184**, 234-242. doi:10.1016/j.exer.2019.05.001

Wan, Y., Otsuna, H., Chien, C. B. and Hansen, C. (2012). FluoRender: an application of 2D image space methods for 3D and 4D confocal microscopy data visualization in neurobiology research. *IEEE Pac Vis Symp* 201-208. doi:10.1109/pacificvis.2012.6183592

Wan, Y., Otsuna, H., Holman, H. A., Bagley, B., Ito, M., Lewis, A. K., Colasanto, M., Kardon, G., Ito, K. and Hansen, C. (2017). FluoRender: joint freehand segmentation and visualization for many-channel fluorescence data analysis. *BMC Bioinformatics* **18**, 280. doi:10.1186/s12859-017-1694-9

Wang, W., Lo, P., Frasch, M. and Lufkin, T. (2000). Hmx: an evolutionary conserved homeobox gene family expressed in the developing nervous system in mice and Drosophila. *Mech. Dev.* **99**, 123-137. doi:10.1016/S0925-4773(00)00488-3

Warren, J. T., Jr, Chandrasekhar, A., Kanki, J. P., Rangarajan, R., Furley, A. J. and Kuwada, J. Y. (1999). Molecular cloning and developmental expression of a zebrafish axonal glycoprotein similar to TAG-1. *Mech. Dev.* **80**, 197-201. doi:10.1016/S0925-4773(98)00215-9

Weth, F., Fiederling, F., Gebhardt, C. and Bastmeyer, M. (2014). Chemoaffinity in topographic mapping revisited–is it more about fiber-fiber than fiber-target interactions? *Semin. Cell Dev. Biol.* **35**, 126-135. doi:10.1016/j.semcdb.2014.07.010

Wolman, M. A., Sittaramane, V. K., Essner, J. J., Yost, H. J., Chandrasekhar, A. and Halloran, M. C. (2008). Transient axonal glycoprotein-1 (TAG-1) and laminin-alpha1 regulate dynamic growth cone behaviors and initial axon direction in vivo. *Neural Dev* **3**, 6. doi:10.1186/1749-8104-3-6

Woolfe, A., Goodson, M., Goode, D. K., Snell, P., McEwen, G. K., Vavouri, T., Smith, S. F., North, P., Callaway, H., Kelly, K. et al. (2005). Highly conserved non-coding sequences are associated with vertebrate development. *PLoS Biol.* **3**, e7. doi:10.1371/journal.pbio.0030007

Wotton, K. R., Weierud, F. K., Juárez-Morales, J. L., Alvares, L. E., Dietrich, S. and Lewis, K. E. (2009). Conservation of gene linkage in dispersed vertebrate NK homeobox clusters. *Dev. Genes Evol.* **219**, 481-496. doi:10.1007/s00427-009-0311-y

Xiao, T., Roeser, T., Staub, W. and Baier, H. (2005). A GFP-based genetic screen reveals mutations that disrupt the architecture of the zebrafish retinotectal projection. *Development* **132**, 2955-2967. doi:10.1242/dev.01861

Xu, H. P., Burbridge, T. J., Chen, M. G., Ge, X., Zhang, Y., Zhou, Z. J. and Crair, M. C. (2015). Spatial pattern of spontaneous retinal waves instructs retinotopic map refinement more than activity frequency. *Dev. Neurobiol.* **75**, 621-640. doi:10.1002/dneu.22288

Xu, H. P., Burbridge, T. J., Ye, M., Chen, M., Ge, X., Zhou, Z. J. and Crair, M. C. (2016). Retinal wave patterns are governed by mutual excitation among starburst amacrine cells and drive the refinement and maintenance of visual circuits. *J. Neurosci.* **36**, 3871-3886. doi:10.1523/JNEUROSCI.3549-15.2016

Yoshikawa, S., Kawakami, K. and Zhao, X. C. (2008). G2R Cre reporter transgenic zebrafish. *Dev. Dyn.* **237**, 2460-2465. doi:10.1002/dvdy.21673

Yoshiura, K., Leysens, N. J., Reiter, R. S. and Murray, J. C. (1998). Cloning, characterization, and mapping of the mouse homeobox gene Hmx1. *Genomics* **50**, 61-68. doi:10.1006/geno.1998.5284

Zhang, J., Ackman, J. B., Xu, H.-P. and Crair, M. C. (2011). Visual map development depends on the temporal pattern of binocular activity in mice. *Nat. Neurosci.* **15**, 298-307. doi:10.1038/nn.3007